Derivation of the dispersion relation of spin-waves and their off-resonant detection using NV centers in diamond

Nina Simon

5144744

Bachelor thesis

To be defended on Friday 3 Januari, 2023 at 14:00

Supervisors:
T. van der Sar, P. Visser, A. Teepe
Evaluation comittee:
T. van der Sar, P. Visser
M. Blaauboer, W. Groenevelt

Delft, 27 Januari 2023

Abstract

Spin-waves, the propagation of circular preccession of spins, have been offered as a way to replace electric currents as information carriers. The overwhelming advantage being the lack of moving charges and Ohmic losses. In this context, the search for an efficient method of detection of becomes crucial. Nitrogen vacancy centers in diamond offer a highly sensitive and effective solution. These diamond lattice defects have quantum and optical features allowing them to be used to quantify the surrounding magnetic field. This project is composed of a theoretical study of spin waves followed by an experimental section where AC magnetometry is tried out as a detection method. First the computations for the dispersion relation of spin waves in a ferromagnetic material where done. A simplified version assuming homogeneity in one direction is presented and then an expansion considering a wave mode of the first order in the previously constant direction is attempted. An analysis on the efficiency of spin wave generation outlines the conditions on the wavelength and the polarisation needed to correctly drive spin waves while being able to measure them using NV centers. Then the experimental setup and steps of AC magnetometry are layed out. The results of a measurement are shown and are in alignment with the theoretical predictions, proving this to be a valid method.

Contents

1 Introduction

The discovery of spin waves has brought forth a new way to encrypt and transport information by encoding it in the spin of an electron. This science called *Spintronics* [4] offers the advantage of absence of Ohmic losses due to charge movement, which would be a great advantage in the quest to faster computing times. Spin waves are the propagation of a precessional motion of spins through a magnetic insulator. The study of these waves is called *Magnonics*, based on the name of the spin wave quanta *magnons*.

When developing this new way of information it is in our interest to learn to detect the spin waves as they propagate through a material. In this project, NV magnetometry, is looked at as high sensitivity way to detect spin waves using quantum sensors in diamond [12]. NV (for nitrogen vacancy) centers are defects that can be etched into diamond that display quantum properties (they have spin S=1) sensitive to the surrounding magnetic field. The optical dependance of the quantum states allows us to use the photo-luminescence (or PL) of the NV centers as a quantifier. They have been proven to be great magnetometers in a 0-100 MHz frequency range and in many research fields. In this instance they are used to detect and quantify the magnetic field generated by spin waves and subsequently the spin waves themselves. One of the complications of NV sensing, in the 1-100 GHz frequency band of spin waves, in it's simplest form is that it relies on tuning a strong external magnetic, that can alter the properties of the waves, to a specific resonant frequency of the NV spin (the ESR frequency). To remedy this an off-resonant detection method called difference-frequency generation is used.

In our experiments spin waves are generated by induction using a microwave current sent through a gold strip line laid on top of a YIG (Yttrium iron garnet) sample. This material is used as it has a low Gilbert damping factor allowing the spin waves to spread. A square diamond piece containing NV centers is placed on top of the sample. A laser is used to stimulate the PL needed for the detection.

In this paper a first approach to understanding spin-waves is made by exploring the computations leading to the dispersion relation associated with them in YIG and in Permalloy. A reproduction of the computations made in previous papers is done and an attempt to complete them by adding a dimension to the problem is presented. An analysis on how to efficiently generate spin waves in our sample is also done. The second part of the project is an experimental observation of the spin waves and of the detection process associated with them. The looked at technique is AC magnetometry, which is advantageous because it is time sensitive.

2

Magnetometry with NV centers in diamond

The nitrogen-vacancy colour center is a point defect in the diamond crystal lattice. This defect is magnetic and shows quantum behaviour at room temperature. It has electronic spin which can controlled and readout and is also dependant on the magnetic conditions. In this chapter we discuss the nature and properties of the NV centers and how they can be used as powerful magnetometers.

2.1. NV centers in diamonds

Electronic structure

The NV center consists of a nitrogen atom and a vacancy both replacing carbon atoms as in figure 2.1. There are two versions of this defect denoted NV^0 and NV^- respectively with 5 and 6 electrons. The latter is generally used for magnetometry and quantum measurements. In this version 2 electrons are from the nitrogen atom, 3 are lose bonds from the missing carbon atom and the last atom captured from the environment [12]. The neutrally charged state is not magneto-optically active and therefore rarely used in NV experiments. In the rest of this report, the term NV center will refer to the negatively charged state. Because of the lattice symmetry there are 4 possible orientations of the NV centers that are differ from each-other by an angle of 71.

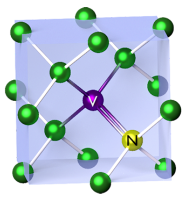

Figure 2.1: **Lattice structure of NV centers within the diamond lattice**. One green carbon atom is replaced with the purple vacancy an one with a nitrogen atom (yellow). There are 4 possible orientations for the NV centers within the crystal lattice.Image from [1]

Spin dependent optical properties

In 2.2 the energy diagram of an NV center is depicted. NV centers have three energy levels; a triplet ground state, an excited triplet state and an intermediate singlet state. The triplet states are further split into three spin levels ($m_s = \pm 1$, $m_s = 0$) because they have spin $S = 1$. The energy difference (or so called "zero-field splitting")between these states is $D = 2.87$ GHz for the ground state and $D_{ex} = 1.42$ GHz for the excited state. Transitions between the states can be driven optically using a green laser exciting the spin state from the ground state to the excited state. Relaxation can occur either radiatively while emitting red photons or non radiatevely via the intermediary singlet state from which subsequent decay happens mostly into the $m_s = 0$ state. The $m_s = 0$ decays non-radiatively less often than the $m_s = \pm 1$ states. The net effect of these properties upon optical pumping is that the system gets initialized in the $m_s = 0$ state and that the photo luminescence is much brighter when in the $m_s = 0$ state.

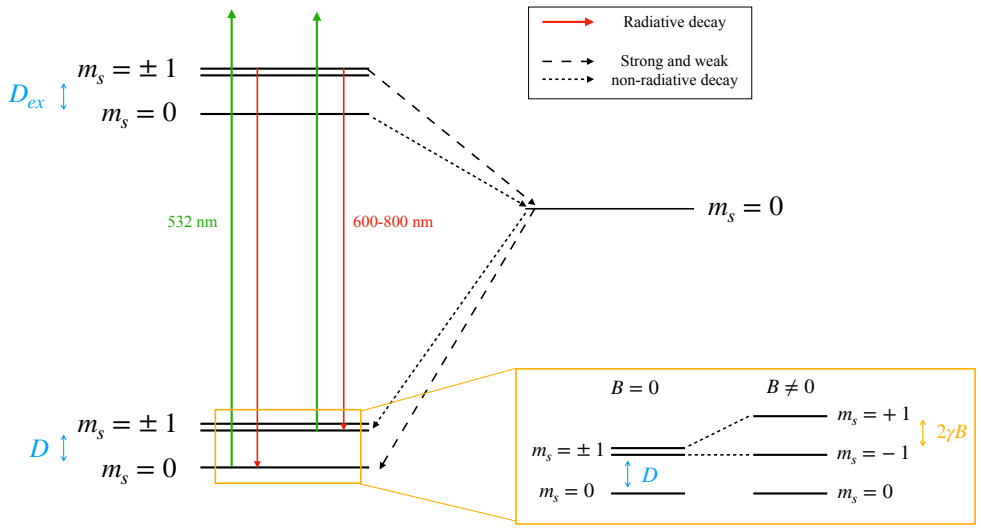

Figure 2.2: **Energy levels of the NV center in diamond**. Optical excitation from the ground state can happen by use of a green laser. Decay can successively happen either radiatively (emitting red light) or non radiatively (no red light emitted) passing by the singlet state. Relaxation from the $m_s = \pm 1$ states is more likely to happen through the singlet state (stronger non radiative decay). When an external magnetic field B is applied the degeneracy of the $m_s = \pm 1$ is lifted by a $2\gamma B$ energy difference. D and $D_e x$ are the zero-field splittings for the ground and excited energy levels. THe green arrows represent the spin-conserving non-resonant optical excitation with a laser with a wavelength of 532nm. The red arrows represent decay via the spin conserving optical transition, here red photons with a $600-800$nm wavelength are emitted.

2.2. NV magnetometry

NV centers are sensitive to the surrounding magnetic fields through their ESR frequency which is dependent on any present static field. An oscillating field at the ESR frequency causes optically detectable transitions of the NV spins. These features form the base of Nv magnetometry. In this chapter we explain the magnetic properties of NV centers.

2.2.1. Electron spin resonance

The simplest NV magnetometry technique is based on the transitions between ms = 0 and ms = ±1 states that happen at certain frequencies. These frequencies are called Electron Spin Resonance (ESR) frequencies. When an oscillating magnetic field at the resonant frequency is applied to the NV centers that where optically initialized into the $m_s = 0$ state, ESR transitions drive the spins into the $m_s = \pm 1$ states. This causes the detected photo luminescence to dip significantly. The ESR frequency is dependent on the presence of a static magnetic field, this feature is used the detect the applied oscillating field.

2.2.2. NV centers in magnetic fields

The magnetic sensing methods are based on the degeneracy lift of the $m_s = \pm 1$ states that happens when a (Static) magnetic field is applied as depicted in 2.2, this is the Zeeman effect. The ESR frequency of an NV center is dependent on the presence of a magnetic field. When there is a magnetic field the Zeeman effect splits the $m_s = \pm 1$ states resulting in the $\omega_\pm$ resonances as shown in figure 2.3. To understand how the magnetic field affects the resonance frequencies one must look at the NV center Hamiltonian [2]:

$$\mathscr{H} = DS_z^2 + \gamma \mathbf{B} \cdot \mathbf{S} \tag{2.1}$$

for an NV center with it's axis along the z direction direction, γ being the electronic gyromagnetic ratio, and $\mathbf{S} = [S_x, S_y, S_z]$ the Paul Spin operators for a spin-1 system and $\mathbf{B}$ a static external magnetic field perfectly aligned with the considered NV center. Here we neglect strains and electric fields. The Hamiltonian in matrix form is then

$$\mathscr{H} = \begin{pmatrix} D + \gamma B_z & \frac{\gamma}{\sqrt{2}}(B_x - iB_y) & 0 \\ \frac{\gamma}{\sqrt{2}}(B_x + iB_y) & 0 & \frac{\gamma}{\sqrt{2}}(B_x - iB_y) \\ 0 & \frac{\gamma}{\sqrt{2}}(B_x + iB_y) & D - \gamma B_z \end{pmatrix} \tag{2.2}$$

notice that the magnetic field causes the shift in the eigenfrequencies of the Hamiltonian which are $\omega_{\pm} = D \pm \gamma B_z$. As said before this is only the case for NV centers aligned with the magnetic field, other families experience a transverse field. When a magnetic field is present there are two ESR dips which are separated by a $2\gamma B$ frequency difference, measuring this difference therefore allows a qualitative estimate of the magnetic field. In figure 2.3 an ESR measurement plot is shown. Two distinct dips in photo-luminescence are apparent and match with the predicted ESR frequencies. ‘

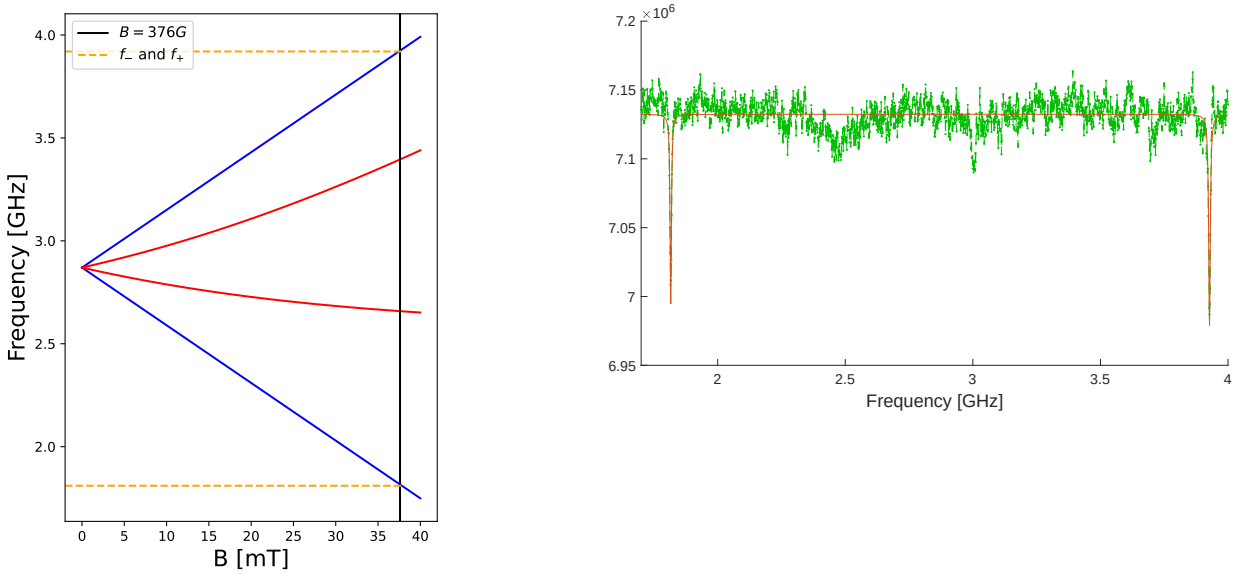

(a) (b)

Figure 2.3: **ESR frequencies predicted and measured (a)** ESR frequencies versus the external static magnetic field when the field is aligned with the magnetic field (blue lines) and for the three other families (red lines) which are degenerate and experience the same field. Here the energy difference due to Zeeman splitting is apparent. The black line marks the $B = 376G$ point on the horizontal axis to compare the theoretical ESR frequencies with the ones measured in (b). **(b)** ESR measurement done with presence of a static magnetic field of 376 G. On the x-axis the frequency of the applied microwave field which is swept across frequencies around the resonant frequency. On the y-axis we have the counts per seconds, or the measured red photo-luminescence coming from the NV centers in the observed sample. The data is fitted to determine the frequency of the ESR dips. We observe two dips, one at 1.8160(2) GHz and one at 3.9273(2) GHz which match with f and f_+ as predicted in figure (a).

2.2.3. Measuring Rabo oscillations to quantify oscillating magnetic fields

In order to quantify the oscillating magnetic field generated by the spin waves so called ’Rabi’ oscillations are measured. When a resonant magnetic field is applied to the NV centers, it’s state coherently oscillates between the $m_s = 0$ and the $m_s = \pm 1$ states (depending on the chirality of the magnetic field) with the frequency given by [2]:

$$\Omega_R = \gamma \frac{B_{AC}}{\sqrt{2}} \tag{2.3}$$

assuming the oscillating magnetic field is B_{AC}. This process is schematized in figure 2.4. To ensure there is resonance an ESR measurement is always done first. In order to measure Rabi oscillations a pulsed control scheme is applied: the spins are first initialized in the $m_s = 0$ state with a laser pulse, microwave of increasing duration rotate the Nv spin between the $m_s = 0$ and the $m_s = \pm 1$ states. The Rabi frequency and thus the magnitude of the oscillating magnetic field can be deduced from the period of the luminescence oscillations.

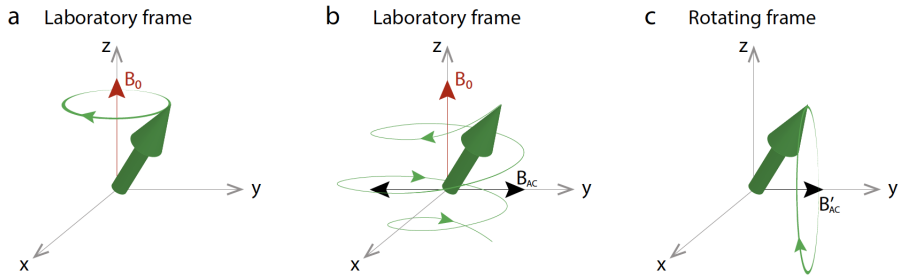

Figure 2.4: **Schematizations of electron spin in a magnetic field**. (a) In the laboratory frame the spin precesses around the static magnetic field it is subject to. (b) When an oscillating magnetic field is applied, the spin precesses around the vector sum of the static magnetic field and the oscillating magnetic field. (c) In a reference frame rotating at the same frequency as the oscillating field, the spin precesses around the transverse field.Figures from [2].

When the Rabi oscillations frequency is known, the length of a π pulse which would prepare the spin in the $m_s = 1$ or $m_s = -1$ state is accessible. Choosing the pulse length corresponding to the first minimum in the luminescence oscillations.

2.2.4. A non-linear mixing method to detect broader frequency bands

A big limitation of the previously explained NV measurement technique is that it relies on tuning the external magnetic field to select the needed ESR frequency to detect the external magnetic field we are trying to detect. This limits the range of detectable frequencies. To broaden this range would require big external magnetic fields which are not realisable experimentally. A solution used to remedy this implies the detection of off resonant frequencies. In the measurements described further in the paper the Difference-frequency generation method is used. Here the target signal frequency f_s is locally converted to the NV spin resonance frequency by mixing with a 'pump' frequency f_p and therefore becomes detectable. When the difference frequency $|f_s - f_p|$ becomes equal to the NV ESR frequency the transverse magnetization experiences a beating and a dip in photoluminence is perceivable making f_s an accessible quantity.

2.2.5. AC magnetometry

AC magnetometry [5] is a time sensitive measurement method for the oscillating magnetic field generated by the spin waves. It uses a series of well timed π and $\pi/2$ pulses creating a phase difference to the situation where there is no oscillating field which translates into a population difference and therefore to a photoluminescence difference. This phase difference is proportional to the amplitude of the magnetic field we are trying to measure by the relation:

$$\Delta\theta \propto \gamma B_{AC} T \tag{2.4}$$

where T is the total evolution time of the used measurement sequence. The measurement technique is illustrated in figure using a Bloch sphere : the spin is initialized in the $m_s = 0$ state by a laser pulse which is along the z-axis on the Bloch sphere. A $\pi/2$ pulse is applied getting the spin into the xy plane of the Bloch sphere where it oscillates (therefore it's phase oscillates) if an oscillating magnetic field is present. The phase difference is maximized by applying a series of π pulses as the spin is at one of the extremities of it's oscillations (when at a half period). A final $\pi/2$ pulse gets the spin out of the xy plane ready to be readout. Because of the dephasing not as many spins will be in the $m_s = 0$ state causing a contrast in PL. The measurements are made by variating the time τ between the π pulses, when this matches a half period of the oscillating field we should observe a maximal contrast in photoluminescence.

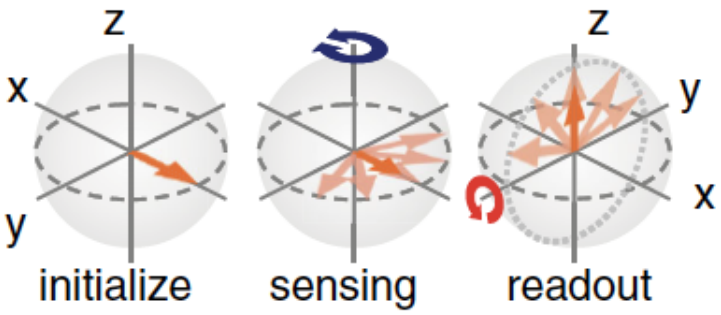

Figure 2.5: **Spin manipulations made during an AC magnetometry measurment**. In the left most image the spin in initialized and move to the xy plane by a $\pi/2$ pulse. In the center figure the spin starts dephasing because of the oscillating magnetic field, the averaged phase difference is nul. It is in the 'sensing' phase that a series of π pulses are applied. On the left the spin has been flipped back to the yz plane before the readout, there is now a population difference. Image taken from [5]

3

Spin waves theory

Spin waves are a propagating disturbance in magnetic materials. The spins in the material are aligned along the magnetic field, this is their equilibrium position. A disturbance can appear or be driven by an oscillating magnetic field, the spin will precess around it's equilibrium position. Since the neighbouring spins are coupled by the exchange and dipolar interactions this excitation can propagate by exchanging torque with it's neighbour spins. The frequencies of these waves range from GHz to THz. A schematisation of this wave is shown in figure 3.1. In this section the dispersion relation the spin waves propagating through thin ferromagnetic films (either YIG or Permalloy) is derived. The situation is analyzed were the external bias field is taken in the z direction such that $\mathbf{B_0} = B_0\hat{z}$. In this report the eventual out of plane components of the magnetic field are neglected, since the effect of the out of plane components can be neglected and we take the on plane projection of B_0 as the field. We will also look at how the spin waves in the sample can be efficiently generated considering the setup that is used in the measurements.

3.1. Magnetization dynamics as described by the Landau-Lifshitz-Gilbert equation

In this section an analysis of the dynamics of the magnetization within a thin Ytrium iron garnet film (or YIG) sample is done. YIG is often used in spin-wave research because of it's low gilbert damping $\alpha_{YIG} = 2.7(5) \times 10^{-5}$ [2]. The situation is sketched in figure 3.2; the sample lays in the lab reference frame within a static magnetic field B_0. We study the magnetization denoted **M** as function of time and space. **k** (for an overview of the characters and definitions see the annex) is the wave vector and it makes angle ϕ with the regards to the equilibrium magnetization. Which is described by the Landau-Lifshitz-Gilbert (LLG) equation as defined by

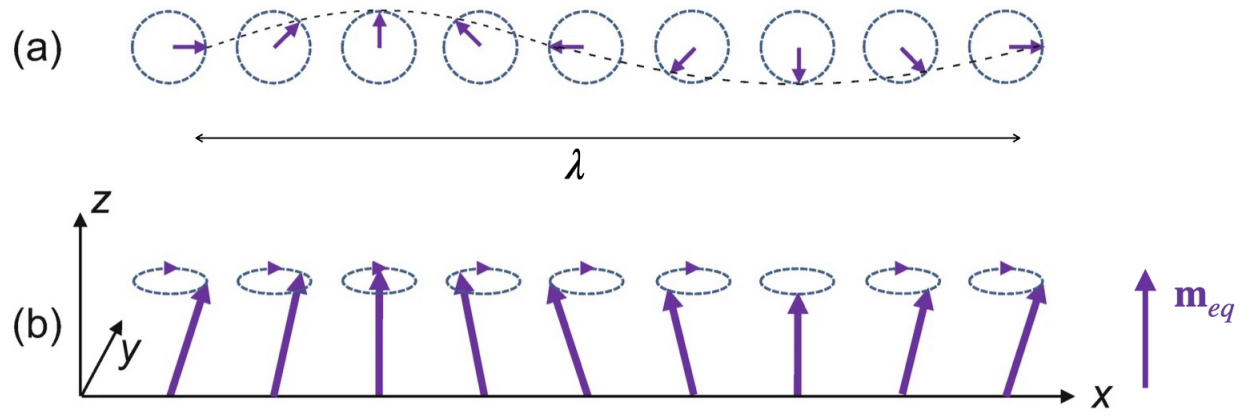

Figure 3.1: **Visualisation of a spin wave adapted from [11]**. The neighbouring spins's magnetization precess around their equilibirum position $\mathbf{m}_{\text{eq}}$ each with slight phase difference resulting in a wave with wavelength λ.

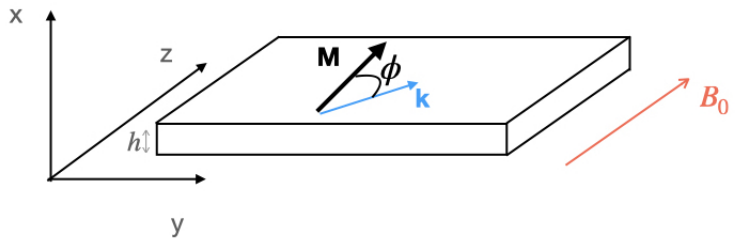

Figure 3.2: **Geometry of the sample**. A thin film of the sample in the yz plane with an external magnetic field B_0 applied along the z-axis. The spin waves propagate through the sample in the **k** direction with an angle ϕ with regards to the magnetization **M**. The unit vectors are defined as $\mathbf{e_x}$,$\mathbf{e_y}$,$\mathbf{e_z}$.

Gilbert [6]:

$$\frac{\partial \mathbf{M}}{\partial t} = -\gamma \mathbf{M} \times (\mathbf{B_{eff}} + \mathbf{B_{AC}}) - \frac{\alpha_G}{M_s} \dot{\mathbf{M}} \times \mathbf{M}, \tag{3.1}$$

We will look at the unit moment $\mathbf{m} = \frac{\mathbf{M}}{M_s}$

$$\frac{\partial \mathbf{m}}{\partial t} = -\gamma \mathbf{m} \times (\mathbf{B_{eff}} + \mathbf{B_{AC}}) - \alpha_G \dot{\mathbf{m}} \times \mathbf{m}, \tag{3.2}$$

where $\mathbf{B_{eff}}$ is the effective magnetic field which is elaborated further and $\mathbf{B_{AC}}$ is the drive field used to generate

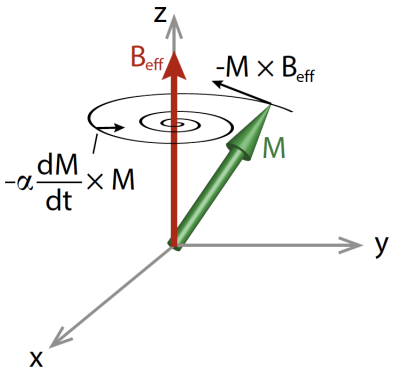

Figure 3.3: **Magnetization dynamics of the spins within a ferromagnetic material with Gilbert damping α in an effective field $B_{\mathbf{eff}}$**. This schematisation shows the action of the two terms in the LLG equation on the variation of the magnetization. The term $-\alpha_G \frac{\mathrm{d}\mathbf{M}}{\mathrm{d}t} \times \mathbf{M}$ accounts for the damping of the magnetization towards the effective field and $-M \times B_{\mathrm{eff}}$ creates the precession movement of the magnetization. Image taken from [2]

the spin waves in the sample. The constants are the electron gyromagnetic ratio γ ratio and α_G, the Gilbert damping. M_s is the saturation magnetization which is dependant on the material. As shown in figure 3.3 the first term in the equation describes the precession of the magnetization around it's equilibrium position while the second term accounts for the damping of the precession towards the equilibrium position. The effective magnetic field is resulting from all the magnetic interactions taking place within the sample which are described by the magnetic free energy density F;

$$F = -M_s \mathbf{m} \cdot \left(\mathbf{B_0} + \frac{\mathbf{B}_\mathrm{D}}{2} \right) + \frac{D}{2} \sum_{\alpha,\beta=x,y,z} \left(\frac{\partial m_\alpha}{\partial \beta} \right)^2. \tag{3.3}$$

This equation gives the following effective magnetic field

$$\mathbf{B}_{\mathrm{eff}} = \mathbf{B}_0 + \mathbf{B}_\mathrm{D} + \mathbf{B}_{\mathrm{ex}} \tag{3.4}$$

The contribution of an anisotropy energy is in this report neglected considering the materials we are using in the experiments (YIG and permalloy) are "soft magnetic materials", the anisotropy is minimized within these

samples and it is a fair assumption to neglect the effects in our computations. The contributions of the other interactions coming forth in the free density energy are further elaborated in the following sections.

Zeeman energy

The static magnetic bias field $\mathbf{B_0}$ causes a Zeeman effect which results in the following energy:

$$F_Z = -M_s \mathbf{m} \cdot \mathbf{B_0} \tag{3.5}$$

with M_s the saturation magnetization of the studied sample. We define $\omega_0 = B_0\gamma$ to simplify the following computations.

Demagnetizing field

The demagnetizing field can be interpreted as the way the spins reacts to the dipolar field caused by surrounding spins. The magnetic field generated by a magnetization $M_s\mathbf{m}(\mathbf{r})$ is given by Ref. [8]

$$\mathbf{B}_\mathrm{D}(\mathbf{r}) = \mu_0 M_s \int \Gamma\left(\mathbf{r}-\mathbf{r}'\right)\mathbf{m}(\mathbf{r}')\mathrm{d}\mathbf{r}' \tag{3.6}$$

Where $\Gamma(\mathbf{r})$ is the dipolar tensor with derivatives of the "Coulomb kernel" as components.

$$\Gamma_{\alpha,\beta}(\mathbf{r},\mathbf{r}') = \frac{\partial^2}{\partial\alpha\partial\beta'}\frac{1}{4\pi\left|\mathbf{r}-\mathbf{r}'\right|}, \quad \text{with} \quad \alpha,\beta = x,y,z \tag{3.7}$$

The 2D Fourrier transform[1] of the magnetic field is:

$$\mathbf{B}_\mathrm{D}(x,\mathbf{k}) = \mu_0 M_s \int \Gamma(\mathbf{k}, x-x')\mathbf{m}(\mathbf{k},x')\mathrm{d}x' \tag{3.8}$$

where $\mathbf{k} = (k_y, k_z)$ as shown in figure 3.2. Assuming the magnetization is homogeneous through the thickness of the sample we define the following

$$\mathbf{m}(x,y,z) = \begin{cases} \mathbf{m}(y,z) & \text{for } -h < x < 0 \\ 0 & \text{elsewhere} \end{cases} \tag{3.9}$$

And thus $\mathbf{m}(\mathbf{k})$ is the Fourrier transform of $\mathbf{m}(y,z)$ within the sample. Inserting this notation into equation 3.8 gives when averaged over the film thickness

$$\overline{\mathbf{B}_\mathrm{D}(\mathbf{k})} = \frac{\mu_0 M_s}{h}\int_{-h}^{0}\int_{-h}^{0}\Gamma(\mathbf{k}, x-x')\mathrm{d}x\mathrm{d}x'\mathbf{m}(\mathbf{k}). \tag{3.10}$$

Using the identity

$$\frac{1}{|\mathbf{r}-\mathbf{r}'|} = \frac{1}{2\pi}\int \frac{e^{-k|x-x'|}}{k} e^{i\mathbf{k}\cdot(\rho-\rho')}\mathrm{d}^2\mathbf{k} \tag{3.11}$$

with $\boldsymbol{\rho} = x\hat{\mathbf{x}} + y\hat{\mathbf{y}}$ and $\mathbf{m}(\mathbf{k})$ is the 2D Fourrier transform of $m(y,z)$ the components of the dipolar tensor in Fourrier space can be derived giving:

$$\Gamma_{\alpha,\beta}(x,k_y,k_z) = \frac{1}{2}\begin{cases} -e^{-k|x-x'|}k - 2\delta(x-x') & \text{for} \quad \alpha=\beta=x, \\ -e^{-k|x-x'|}\frac{k_\alpha k_\beta}{k} & \text{for} \quad \alpha,\beta = y,z, \\ -ik_\beta e^{-k|x-x'|}\mathrm{sign}(x-x') & \text{for} \quad \alpha = x \quad \text{and} \quad \beta = y,z \\ -ik_\alpha e^{-k|x-x'|}\mathrm{sign}(x-x') & \text{for} \quad \alpha = y,z \quad \text{and} \quad \beta = x \end{cases} \tag{3.12}$$

which when inserted into 3.10 gives the final formula

$$\overline{\mathbf{B_D}(\mathbf{k})} = \mu_0 M_s \begin{pmatrix} f-1 & 0 & 0 \\ 0 & -\frac{k_y^2}{k^2}f & -\frac{k_y k_z}{k^2}f \\ 0 & -\frac{k_y k_z}{k^2}f & -\frac{k_z^2}{k^2}f \end{pmatrix}\mathbf{m}(\mathbf{k}) = \mu_0 M_s \begin{pmatrix} f-1 & 0 & 0 \\ 0 & -\sin^2\phi f & -\sin\phi\cos\phi f \\ 0 & -\sin\phi\cos\phi f & -\cos^2\phi f \end{pmatrix}\mathbf{m}(\mathbf{k}) \tag{3.13}$$

where $f = 1 - \frac{1-e^{-kh}}{kh}$ with h the thickness of the film and ϕ is as defined in figure 3.2 the in plane angle between the wave vector and the magnetization, we also define $\omega_D = \gamma\mu_0 M_s$.

[1] Here the 2D Fourrier transform is defined as $\mathscr{F}\{f(\mathbf{k})\} = \int_{-\infty}^{\infty}\int_{-\infty}^{\infty} f(\mathbf{r})e^{-ik_y y - ik_z z}dydz$ with inverse transform $f(\mathbf{r}) = \frac{1}{4\pi^2}\int_{-\infty}^{\infty}\int_{-\infty}^{\infty}\mathscr{F}\{f(\mathbf{k})\}e^{ik_y y + ik_z z}dk_y dk_z$. In this paper we use the notation $f(\mathbf{k})$ as the 2D Fourrier transform in the sample plane.

Exchange energy

The exchange energy for an isotropic sample (like Yttrium-Iron-Garnet or Permalloy) is given by,

$$F_{\text{ex}}(\mathbf{r}) = \frac{D}{2} \sum_{\alpha,\beta=x,y,z} \left(\frac{\partial m_\alpha}{\partial \beta} \right)^2 \tag{3.14}$$

where D is the spin stiffness [3]. The 2D Fourrier transform of this energy over the yz plane is

$$F_{\text{ex}}(x,\mathbf{k}) = -\frac{D}{2} k^2 \left(m_y^2(x,\mathbf{k}) + m_z^2(x,\mathbf{k}) \right) + \frac{D}{2} \sum_{\alpha=x,y,z} \left(\frac{\partial m_\alpha(x,\mathbf{k})}{\partial x} \right)^2 \tag{3.15}$$

In the following computations we assume a constant magnetization through the film thickness (in the x direction). This is however not necessarily true as spin wave modes can appear in the x direction. This will be explained later in the report. For now, with constant magnetisation in the x direction, the exchange energy therefore contributes an effective field which is zero in the x direction and for the y an z coordinates is:

$$B_{\text{ex},\alpha}(\mathbf{k}) = -\frac{1}{M_s} \frac{\partial F}{\partial m_\alpha} = -\frac{\omega_{\text{ex}}}{\gamma} k^2 m_\alpha(\mathbf{k}), \quad \text{with} \quad \alpha = y,z \tag{3.16}$$

$$B_{\text{ex},x} = 0 \tag{3.17}$$

Where $\omega_{\text{ex}} = \gamma D / M$.

3.1.1. Dispersion relation and susceptibility

We assume a weak response of the spins in the xy plane, thus we can make the following approximation: $m_z = \sqrt{1 - m_x^2 - m_y^2} \approx 1$. Linearizing the LLG equation 3.2 and taking the Fourrier transform over time[2]:

$$\begin{aligned} -i\omega m_x &= -\gamma(m_y B_z - B_y m_z) + i\omega\alpha m_y \\ -i\omega m_y &= -\gamma(B_x m_z - m_x B_z) - i\omega\alpha m_x \end{aligned} \tag{3.18}$$

Where $\mathbf{B} = \mathbf{B}_{eff} + \mathbf{B}_{AC}$ taking into account the contributions of the magnetic fields within the samples gives

$$\begin{aligned} \gamma B_x &= \omega_D (f-1) m_x - \omega_{\text{ex}} k^2 m_x + \gamma B_{AC,x} \\ \gamma B_y &= -\omega_D \sin\phi^2 f m_y - \omega_{\text{ex}} k^2 m_y + \gamma B_{AC,y} \\ \gamma B_z &= \omega_0 \end{aligned} \tag{3.19}$$

where higher order terms of the magnetization (like m_y^2) are neglected. Defining

$$\begin{aligned} \omega_1 &= \omega_0 + \omega_{\text{ex}} k^2 \\ \omega_2 &= \omega_1 + \omega_D (1-f) \\ \omega_3 &= \omega_1 + \omega_D f \sin^2\phi \end{aligned} \tag{3.20}$$

we get the linearized equation in matrix form:

$$\begin{pmatrix} \omega_2 - i\alpha\omega & i\omega \\ -i\omega & \omega_3 - i\alpha\omega \end{pmatrix} \begin{pmatrix} m_x \\ m_y \end{pmatrix} = \gamma \begin{pmatrix} B_{AC,x} \\ B_{AC,y} \end{pmatrix} \tag{3.21}$$

Inverting this equation get us the form $\mathbf{m} = \chi \mathbf{B}_{AC}$ which describes how the system reacts to the applied microwave drive field B_{AC}. χ is the susceptibility and is a Lorentzian function of ω which peaks around its resonance frequency and the width of the peak is dictated by the Gilbert damping factor.

$$\chi = \frac{\gamma}{(\omega_2 - i\alpha\omega)(\omega_3 - i\alpha\omega) - \omega^2} \begin{pmatrix} \omega_3 - i\alpha\omega & -i\omega \\ i\omega & \omega_2 - i\alpha\omega \end{pmatrix} \tag{3.22}$$

Looking for the resonant frequencies by finding the singularities of the susceptibility:

$$(\omega_2 - i\alpha\omega)(\omega_3 - i\alpha\omega) - \omega^2 = 0 \tag{3.23}$$

[2] In this case we go from time to frequency domain with $\mathscr{F}\{f(\mathbf{t})\} = \int_{-\infty}^{\infty} f(\mathbf{t}) e^{-i\omega t} dt$ with inverse transform $f(\mathbf{r}) = \frac{1}{2\pi} \int_{-\infty}^{\infty} \mathscr{F}\{f(\mathbf{t})\} e^{i\omega t} d\omega$

finding the complex solutions for ω

$$\omega = -i\alpha\frac{\omega_2+\omega_3}{2\left(1+\alpha^2\right)} + \sqrt{\frac{\omega_2\omega_3}{1+\alpha^2} - \frac{\alpha^2(\omega_2+\omega_3)^2}{4\left(1+\alpha^2\right)^2}} \tag{3.24}$$

the spin-wave dispersion appears. For small Gilbert damping we can neglect α^2 terms

$$\omega_{sw} \approx \sqrt{\omega_2\omega_3} \tag{3.25}$$

and the spin wave line-width is:

$$\Delta\omega_{sw} \approx \frac{\alpha\left(\omega_2+\omega_3\right)}{2} \tag{3.26}$$

Some cases are interesting to highlight and relate to the dispersion relation:

- When the the spin waves propagates in direction transverse to the magnetization (or $\phi = \pi/2$), we talk about the Damon-Eshbach (or DE) regime. The DE dispersion relation is

$$\omega_{sw} = \sqrt{\left(\omega_1 + f\omega_D\right)\left(\omega_1 + (1-f)\omega_D\right)} \tag{3.27}$$

- When the the spin waves propagates in the magnetization direction (or $\phi = 0$), we talk about the Backward-Volume (or BV) regime because of the negative group velocity in this case. The BV dispersion relation is

$$\omega_{sw} = \sqrt{\omega_1\left(\omega_1 + (1-f)\omega_D\right)} \tag{3.28}$$

- The situation where $k = 0$ is the ferromagnetic resonance mode (FMR).

$$\omega_{sw} = \sqrt{\omega_0\left(\omega_0 + \omega_D\right)} \tag{3.29}$$

The DE and BV dispersion relations are plotted in 3.4. The spin waves considered in the experiments performed in the lab are in the DE regime.

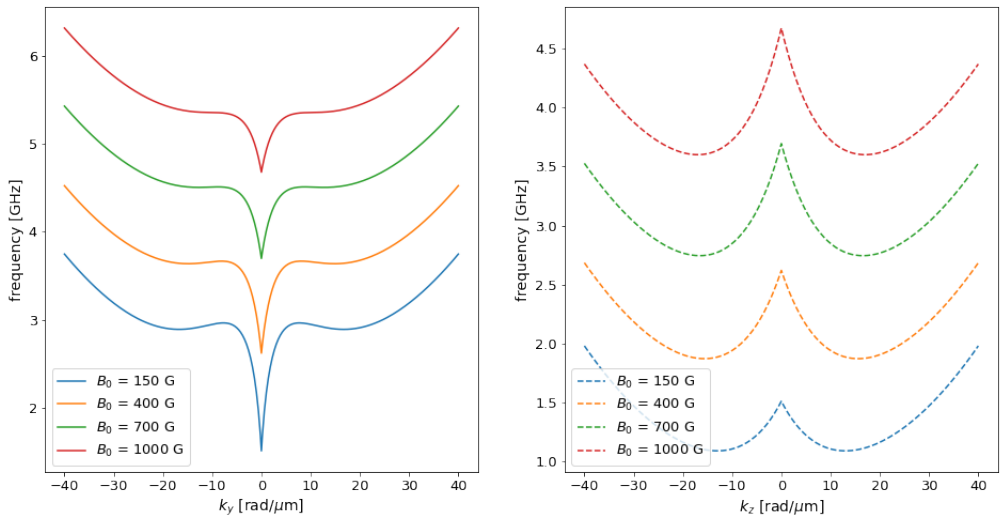

Figure 3.4: **Calculated spin wave dispersion for YIG film**. The thickness was taken to be 235nm with saturation magnetization $M_s = 1.42 \times 10^5$ A/m. On the left the Damon-Eshbach spin waves propagating in the y direction and on the right the Backwards-Volume spin waves propagating in the z direction. Notice that the FMR point gets higher with higher magnetic field.

3.2. Dispersion relation with transversal modes

Spin waves mostly exist in the sample plane but at some frequencies will appear in the thickness direction of the film due to scattering into the first transversal spin mode. This effect has been observed during NV measurements of spin waves in the lab as can be seen in figure 3.5, where a decrease in photo luminescence on the ESR axis is seen. In this chapter a method to include the spin wave modes appearing in the thickness direction of the YIG sample is presented. It is an attempt to simplify the calculations made in [10] using a similar method as in the previous chapter. First analyzing the situation with 'pinned' surface spins and then 'unpinned' surface spins.

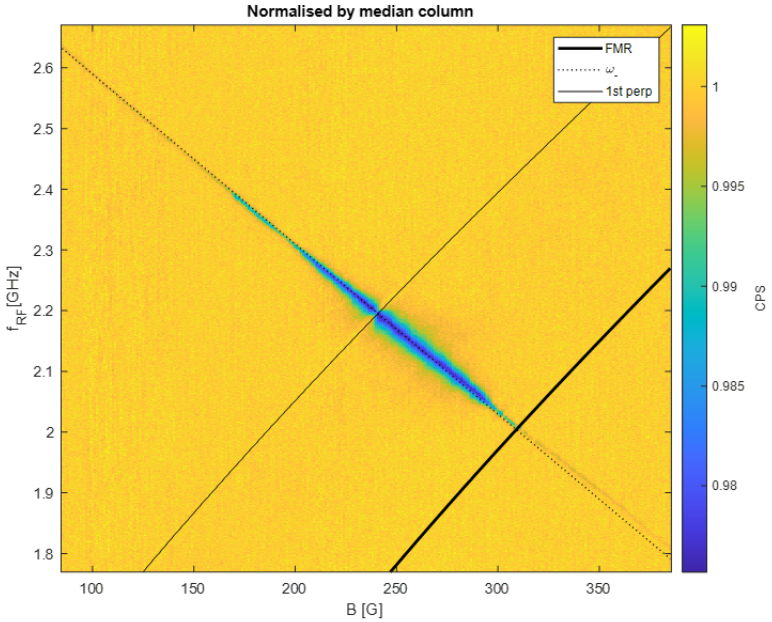

Figure 3.5: **Normalized photo luminescence of a diamond film superposed on a YIG sample as a function of the microwave (thus spin wave frequency) and the static magnetic field**. The theoretical ESR is given by the dotted line and the FMR is given by the black line. The appearance of the first transversal mode is marked by the thinner black line.

3.2.1. Pinned surface spins

We first look at the situation where the surface spins are pinned, this is the term used to describe the boundary conditions of the magnetization on the upper and lower edges of the sample in [10]. In the pinned case they are $m_{x=0,-h} = 0$ or zero magnetization at the edges.

Exchange energy

In the same way as previously the 2D Fourrier transform of the Free Exchange energy over the yz plane is

$$F_{\text{ex}}(x,\mathbf{k}) = -\frac{D}{2}k^2\left(m_y^2(\mathbf{k},x) + m_z^2(\mathbf{k},x)\right) + \frac{D}{2}\sum_{\alpha=x,y,z}\left(\frac{\partial m_\alpha(x,\mathbf{k})}{\partial x}\right)^2 \tag{3.30}$$

Now assuming we have a first order mode for the magnetization in the x direction (direction of the thickness) of the sample and as said before pinned edges:

$$\mathbf{m}(x,y,z) = \begin{cases} \mathbf{m}(y,z)\sin\left(\frac{\pi x}{h}\right) & \text{for } -h < x < 0 \\ 0 & \text{elsewhere} \end{cases} \tag{3.31}$$

where $\mathbf{m}(y,z) = m_x(y,z)\hat{\mathbf{x}} + m_y(y,z)\hat{\mathbf{y}} + m_z(y,z)\hat{\mathbf{z}}$. Taking the 2D Fourrier transform on the yz plane:

$$\mathbf{m}(x,\mathbf{k}) = \begin{cases} \mathbf{m}(\mathbf{k})\sin\left(\frac{\pi x}{h}\right) & \text{for } -h < x < 0 \\ 0 & \text{elsewhere} \end{cases} \tag{3.32}$$

with now $\mathbf{m}(\mathbf{k}) = m_x(\mathbf{k})\hat{\mathbf{x}} + m_y(\mathbf{k})\hat{\mathbf{y}} + m_z(\mathbf{k})\hat{\mathbf{z}}$, $m_x(\mathbf{k})$ being the 2D Fourrier transform of $m_x(y,z)$. Inserting this into the Free energy equation we have the following:

$$F_{\text{ex}}(x,\mathbf{k}) = -\frac{D}{2}k^2 \sin^2\left(\frac{\pi x}{h}\right)\left(m_y^2(\mathbf{k}) + m_z^2(\mathbf{k})\right) + \frac{D\pi^2}{2h^2}\cos^2\left(\frac{\pi x}{h}\right)\left(m_x^2(\mathbf{k}) + m_y^2(\mathbf{k}) + m_z^2(\mathbf{k})\right) \tag{3.33}$$

We average the exchange energy over the thickness of the sample

$$F_{\text{ex}}(\mathbf{k}) = \frac{1}{h}\int_{-h}^{0} F_{\text{ex}}(x,\mathbf{k})\,\mathrm{d}x = \frac{-D}{4}k^2\left(m_y^2(\mathbf{k}) + m_z^2(\mathbf{k})\right) + \frac{D\pi^2}{4h^2}\left(m_x^2(\mathbf{k}) + m_y^2(\mathbf{k}) + m_z^2(\mathbf{k})\right) \tag{3.34}$$

using the definition

$$B_{\text{ex},\alpha}(\mathbf{k}) = -\frac{1}{M_s}\frac{\partial F}{\partial m_\alpha}, \quad \text{with} \quad \alpha = x,y,z \tag{3.35}$$

the exchange field is then

$$B_{\text{ex},\alpha} = \begin{cases} -\frac{\omega_{\text{ex}}\pi^2}{2\gamma h^2}m_\alpha(\mathbf{k}) & \text{if } \alpha = x \\ -\frac{\omega_{\text{ex}}}{\gamma}\left(\frac{\pi^2}{2h^2} - \frac{k^2}{2}\right)m_\alpha(\mathbf{k}) & \text{if } \alpha = y,z \end{cases} \tag{3.36}$$

Demagnetizing field

For the demagnetizing field we use the same steps as in the previous section but using assumption 3.31. Equation 3.8 gives

$$\mathbf{B}_{\text{D}}(x,\mathbf{k}) = \mu_0 M_s \int \Gamma\left(x - x',\mathbf{k}\right)\mathbf{m}\left(x',\mathbf{k}\right)\mathrm{d}x' \tag{3.37}$$

Inserting the magnetization from 5.1 into 3.64 we get

$$\mathbf{B}_{\text{D}}(x,\mathbf{k}) = \mu_0 M_s \int_{-h}^{0} \Gamma\left(x - x',\mathbf{k}\right)\sin\left(\frac{\pi x'}{h}\right)\mathrm{d}x'\mathbf{m}(\mathbf{k}) \tag{3.38}$$

We define the following functions in order to simplify the coming computations

$$\epsilon(x,k) = \int_{-h}^{0} e^{-k|x-x'|}\sin\left(\frac{\pi x'}{h}\right)\mathrm{d}x' = \frac{h}{k^2h^2+\pi^2}\left(2kh\sin\left(\frac{\pi x}{h}\right) - \pi e^{-k(x+h)} - \pi e^{kx}\right) \tag{3.39}$$

$$\delta(x,k) = \int_{-h}^{0} e^{-k|x-x'|}\text{sign}(x-x')\sin\left(\frac{\pi x'}{h}\right)\mathrm{d}x' = \frac{h}{k^2h^2+\pi^2}\left(-2\pi\cos\left(\frac{\pi x}{h}\right) - \pi e^{-k(x+h)} + \pi e^{kx}\right). \tag{3.40}$$

we simplify the matrix for the demagnetizing field

$$\mathbf{B}_{\text{D}}(x,\mathbf{k}) = \mu_0 M_s \int_{-h}^{0} \Gamma\left(x - x',\mathbf{k}\right)\sin\frac{\pi x'}{h}\mathrm{d}x'\mathbf{m}(\mathbf{k}) = \tag{3.41}$$

$$\mathbf{B}_{\text{D}}(x,\mathbf{k}) = \frac{\mu_0 M_s}{2}\begin{pmatrix} -k\epsilon(x,k) - 2\sin\left(\frac{\pi x}{h}\right) & -ik_y\delta(x,k) & -ik_z\delta(x,k) \\ -ik_y\delta(x,k) & -\epsilon(x,k)\frac{k_y^2}{k} & -\epsilon(x,k)\frac{k_yk_z}{k} \\ -ik_z\delta(x,k) & -\epsilon(x,k)\frac{k_yk_z}{k} & -\epsilon(x,k)\frac{k_z^2}{k} \end{pmatrix}\mathbf{m}(\mathbf{k}). \tag{3.42}$$

Computing the first mode of the demagnetizing field:

$$\overline{\mathbf{B}_{\text{D}}(\mathbf{k})} = \frac{\mu_0 M_s}{h}\int_{-h}^{0}\int_{-h}^{0}\Gamma\left(x - x',\mathbf{k}\right)\sin\left(\frac{\pi x'}{h}\right)\sin\left(\frac{\pi x}{h}\right)\mathrm{d}x'\mathrm{d}x\mathbf{m}(\mathbf{k}) \tag{3.43}$$

Defining the function

$$\sigma(k) = \frac{1}{h}\int_{-h}^{0}\epsilon(x,k)\sin\left(\frac{\pi x}{h}\right)\mathrm{d}x = \frac{kh^2}{k^2h^2+\pi^2} + \frac{2\pi^2 h}{\left(k^2h^2+\pi^2\right)^2}\left(e^{-hk}+1\right) \tag{3.44}$$

and

$$\mu(k) = \frac{1}{h}\int_{-h}^{0}\delta(x,k)\sin\left(\frac{\pi x}{h}\right)\mathrm{d}x = \frac{2h\pi^2}{\left(k^2h^2+\pi^2\right)^2}\left(e^{-hk}+1\right). \tag{3.45}$$

The final equation for the demagnetizaing field is

$$\overline{\mathbf{B}_{\text{D}}(\mathbf{k})} = \frac{\mu_0 M_s}{2}\begin{pmatrix} -k\sigma(k) - 1 & -ik_y\mu(k) & -ik_z\mu(k) \\ -ik_y\mu(k) & -\sigma(k)\frac{k_y^2}{k} & -\sigma(k)\frac{k_yk_z}{k} \\ -ik_z\mu(k) & -\sigma(k)\frac{k_yk_z}{k} & -\sigma(k)\frac{k_z^2}{k} \end{pmatrix}\mathbf{m}(\mathbf{k}). \tag{3.46}$$

Dispersion relation

Using the same method as before the new susceptibility matrix can be computed. Still considering $m_z = \sqrt{1-m_x^2-m_y^2} \sim 1$ we insert the new effective magnetic field into the LLG equation obtaining

$$\begin{aligned} -i\omega m_x &= -\gamma(m_y B_z - B_y m_z) + i\omega\alpha m_y \\ -i\omega m_y &= -\gamma(B_x m_z - m_x B_z) - i\omega\alpha m_x \end{aligned} \tag{3.47}$$

where the notations are

$$\begin{aligned} \gamma B_x &= -\frac{\omega_{\text{ex}}\pi^2}{2h^2} m_x - \frac{\omega_D}{2}\left((k\sigma(k)+1)m_x + ik_y\mu(k)m_y + ik_z\mu(k)m_z\right) + \gamma B_{AC,x} \\ \gamma B_y &= -\omega_{\text{ex}}\left(\frac{\pi^2}{2h^2} - \frac{k^2}{2}\right)m_y - \frac{\omega_D}{2}\left(ik_y\mu(k)m_x + \sigma(k)\frac{k_y^2}{k}m_y + \sigma(k)\frac{k_y k_z}{k}m_z\right) + \gamma B_{AC,y} \\ \gamma B_z &= \omega_0 - \omega_{\text{ex}}\left(\frac{\pi^2}{2h^2} - \frac{k^2}{2}\right)m_z - \frac{\omega_D}{2}\left(ik_z\mu(k)m_x + \sigma(k)\frac{k_y k_z}{k}m_y + \sigma(k)\frac{k_z^2}{k}m_z\right). \end{aligned} \tag{3.48}$$

In the linear regime we neglect higher order terms like m_x^2, m_y^2, m_z^2 and $m_y m_x$ yielding the following equations

$$\begin{aligned} -i\omega m_x &= -\omega_0 m_y + \frac{\omega_D}{2}\left(\sigma(k)\frac{k_z^2}{k}m_y - ik_y\mu(k)m_x - \sigma(k)\frac{k_y^2}{k}m_y\right) + \gamma B_{AC,y} + i\omega\alpha m_y \\ -i\omega m_y &= \omega_0 m_x + \frac{\omega_D}{2}\left((k\sigma(k)+1)m_x + ik_y\mu(k)m_y - \sigma(k)\frac{k_z^2}{k}m_x\right) + \frac{\omega_{\text{ex}}k^2}{2}m_x - \gamma B_{AC,x} - i\omega\alpha m_x \end{aligned} \tag{3.49}$$

which can be rewritten for easier transcription to a matrix

$$\begin{aligned} m_x\left(-i\omega + i\frac{\omega_D}{2}k_y\mu(k)\right) + m_y\left(\omega_0 - \frac{\omega_D}{2}\left(\sigma(k)\frac{k_z^2}{k} - \sigma(k)\frac{k_y^2}{k}\right) - i\omega\alpha\right) &= \gamma B_{AC,y} \\ m_y\left(-i\omega - i\frac{\omega_D}{2}k_y\mu(k)\right) + m_x\left(-\omega_0 - \frac{\omega_D}{2}\left(k\sigma(k) + 1 - \sigma(k)\frac{k_z^2}{k}\right) - \frac{\omega_{\text{ex}}k^2}{2} + i\omega\alpha\right) &= -\gamma B_{AC,x} \end{aligned} \tag{3.50}$$

Defining the following

$$\begin{aligned} \omega_1' &= \frac{\omega_D}{2}k_y\mu(k) \\ \omega_2' &= \omega_0 + \frac{\omega_{\text{ex}}k^2}{2} + \frac{\omega_D}{2}\left(k\sigma(k) + 1 - \sigma(k)\frac{k_z^2}{k}\right) \\ \omega_3' &= \omega_0 - \frac{\omega_D}{2}\left(\sigma(k)\frac{k_z^2}{k} - \sigma(k)\frac{k_y^2}{k}\right) \end{aligned} \tag{3.51}$$

we get the same form as in chapter 3.1 from which we want to exclude the susceptibility $\mathbf{m} = \chi\mathbf{B}_{\text{AC}}$:

$$\begin{pmatrix} \omega_2' - i\alpha\omega & i(\omega_1' + \omega) \\ i(\omega_1' - \omega) & \omega_3' - i\alpha\omega \end{pmatrix}\begin{pmatrix} m_x \\ m_y \end{pmatrix} = \gamma\begin{pmatrix} B_{AC,x} \\ B_{AC,y} \end{pmatrix} \tag{3.52}$$

.

$$\chi' = \frac{\gamma}{\left(\omega_2' - i\alpha\omega\right)\left(\omega_3' - i\alpha\omega\right) + \omega_1'^2 - \omega^2}\begin{pmatrix} \omega_3' - i\alpha\omega & -i(\omega + \omega_1') \\ i(\omega - \omega_1') & \omega_2' - \alpha\omega \end{pmatrix} \tag{3.53}$$

Solving for the singularities:

$$\omega = -i\alpha\frac{(\omega_2+\omega_3)}{2\left(1+\alpha^2\right)} \pm \sqrt{\frac{\omega_2\omega_3 + \omega_1'^2}{1+\alpha^2} - \frac{\alpha^2(\omega_2+\omega_3)^2}{4\left(1+\alpha^2\right)^2}} \tag{3.54}$$

In Yig the damping is very small so we assume $\alpha << 1$:

$$\omega_{\text{sw}}' \approx \sqrt{\omega_2'\omega_3' + \omega_1'^2} \tag{3.55}$$

The dispersion relation in the DE regime is plotted in 3.6.

3.2.2. Unpinned spins on the edges

In this section we look at the situation where the edges are unpinned; with the boundary conditions $\frac{\partial m}{\partial x}_{x=0,-h} = 0$. The 2D Fourrier transform of the Free Exchange energy over the yz plane with $\mathbf{k} = k_y\hat{\mathbf{y}} + k_z\hat{\mathbf{z}}$ and $k = \sqrt{k_y^2 + k_z^2}$ is

$$F_{\text{ex}}(x,\mathbf{k}) = -\frac{D}{2}k^2\left(m_y^2(\mathbf{k},x) + m_z^2(\mathbf{k},x)\right) + \frac{D}{2}\sum_{\alpha=x,y,z}\left(\frac{\partial m_\alpha(x,\mathbf{k})}{\partial x}\right)^2 \tag{3.56}$$

Now assuming we have a first order mode for the magnetization in the x direction (direction of the thickness) of the sample with unpinned edges, that has the following dependence on x:

$$\mathbf{m}(x,y,z) = \begin{cases} \mathbf{m}(y,z)\cos(\kappa_n x) & \text{for } -h < x < 0 \\ 0 & \text{elsewhere} \end{cases} \tag{3.57}$$

where $\kappa_n = \frac{\pi n}{h}$ and $\mathbf{m}(y,z) = m_x(y,z)\hat{\mathbf{x}} + m_y(y,z)\hat{\mathbf{y}} + m_z(y,z)\hat{\mathbf{z}}$. Taking the 2D Fourrier transform on the yz plane:

$$\mathbf{m}(x,\mathbf{k}) = \begin{cases} \mathbf{m}(\mathbf{k})\cos(\kappa_n x) & \text{for } -h < x < 0 \\ 0 & \text{elsewhere} \end{cases} \tag{3.58}$$

with now $\mathbf{m}(\mathbf{k}) = m_x(\mathbf{k})\hat{\mathbf{x}} + m_y(\mathbf{k})\hat{\mathbf{y}} + m_z(\mathbf{k})\hat{\mathbf{z}}$. Inserting this into the Free energy equation we have the following:

$$F_{\text{ex}}(x,\mathbf{k}) = -\frac{D}{2}k^2\cos^2(\kappa_n x)\left(m_y^2(\mathbf{k}) + m_z^2(\mathbf{k})\right) + \frac{D\kappa_n}{2h^2}\sin^2(\kappa_n x)\left(m_x^2(\mathbf{k}) + m_y^2(\mathbf{k}) + m_z^2(\mathbf{k})\right) \tag{3.59}$$

We average the exchange energy over the thickness of the sample

$$F_{\text{ex}}(\mathbf{k}) = \frac{1}{h}\int_{-h}^{0} F_{\text{ex}}(x,\mathbf{k})\,\mathrm{d}x = \frac{-D}{2}k^2\left(m_y^2(\mathbf{k}) + m_z^2(\mathbf{k})\right) + \frac{D\kappa_n^2}{4}\left(m_x^2(\mathbf{k}) + m_y^2(\mathbf{k}) + m_z^2(\mathbf{k})\right) \tag{3.60}$$

using the definition

$$B_{\text{ex},\alpha}(\mathbf{k}) = -\frac{1}{M_s}\frac{\partial F}{\partial m_\alpha}, \quad \text{with} \quad \alpha = x,y,z \tag{3.61}$$

the exchange field is then

$$B_{\text{ex},\alpha} = \begin{cases} -\frac{\omega_{\text{ex}}\pi^2}{2\gamma h^2}m_\alpha(\mathbf{k}) & \text{if } \alpha = x \\ -\frac{\omega_{\text{ex}}}{\gamma}\left(\frac{\pi^2}{2h^2} - \frac{k^2}{2}\right)m_\alpha(\mathbf{k}) & \text{if } \alpha = y,z \end{cases} \tag{3.62}$$

Demagnetizing field

Equation 3.8 gives

$$\mathbf{B}_{\text{D}}(x,\mathbf{k}) = \mu_0 M_s \int \Gamma\left(x - x',\mathbf{k}\right)\mathbf{m}\left(x',\mathbf{k}\right)\mathrm{d}x' \tag{3.63}$$

Inserting the magnetization from 5.1 into 3.64 we get

$$\mathbf{B}_{\text{D}}(x,\mathbf{k}) = \mu_0 M_s \int_{-h}^{0} \Gamma\left(x - x',\mathbf{k}\right)\cos(\kappa_n x)\mathrm{d}x'\mathbf{m}(\mathbf{k}) \tag{3.64}$$

Using these notations

$$\epsilon(x,k) = \int_{-h}^{0} e^{-k|x-x'|}\cos\left(\frac{\pi x'}{h}\right)\mathrm{d}x' = \frac{h^2 k}{k^2h^2 + \pi^2}\left(2\cos\left(\frac{\pi x}{h}\right) + e^{-k(x+h)} - e^{kx}\right) \tag{3.65}$$

$$\delta(x,k) = \int_{-h}^{0} e^{-k|x-x'|}\text{sign}(x-x')\cos\left(\frac{\pi x'}{h}\right)\mathrm{d}x' = \frac{1}{k^2h^2 + \pi^2}\left(2h\pi\sin\left(\frac{\pi x}{h}\right) + kh^2e^{-k(x+h)} + kh^2e^{kx}\right) \tag{3.66}$$

we simplify the matrix for the demagnetizing field

$$\mathbf{B}_{\text{D}}(x,\mathbf{k}) = \mu_0 M_s \int_{-h}^{0} \Gamma\left(x - x',\mathbf{k}\right)\cos\frac{\pi x'}{h}\mathrm{d}x'\mathbf{m}(\mathbf{k}) = \tag{3.67}$$

$$\mathbf{B}_{\text{D}}(x,\mathbf{k}) = \frac{\mu_0 M_s}{2}\begin{pmatrix} -k\epsilon(x,k) - 2\cos\left(\frac{\pi x}{h}\right) & -ik_y\delta(x,k) & -ik_z\delta(x,k) \\ -ik_y\delta(x,k) & -\epsilon(x,k)\frac{k_y^2}{k} & -\epsilon(x,k)\frac{k_yk_z}{k} \\ -ik_z\delta(x,k) & -\epsilon(x,k)\frac{k_yk_z}{k} & -\epsilon(x,k)\frac{k_z^2}{k} \end{pmatrix}\mathbf{m}(\mathbf{k}). \tag{3.68}$$

Computing the first mode of the demagnetizing field:

$$\overline{\mathbf{B}_{\mathrm{D}}(\mathbf{k})} = \frac{\mu_0 M_s}{h}\int_{-h}^{0}\int_{-h}^{0}\Gamma\left(x-x',\mathbf{k}\right)\cos\left(\frac{\pi x'}{h}\right)\mathrm{d}x'\cos\left(\frac{\pi x}{h}\right)\mathrm{d}x\mathbf{m}(\mathbf{k}) \tag{3.69}$$

we find

$$\sigma(k) = \frac{1}{h}\int_{-h}^{0}\epsilon(x,k)\cos\left(\frac{\pi x}{h}\right)\mathrm{d}x = \frac{kh^2}{k^2h^2+\pi^2} - \frac{2h^2ke^{-hk}}{\left(k^2h^2+\pi^2\right)^2}\left(e^{hk}+1\right) \tag{3.70}$$

and

$$\mu(k) = \frac{1}{h}\int_{-h}^{0}\delta(x,k)\cos\left(\frac{\pi x}{h}\right)\mathrm{d}x = 0. \tag{3.71}$$

Thus we have an equation for the demagnetizing field

$$\overline{\mathbf{B}_{\mathrm{D}}(\mathbf{k})} = \frac{\mu_0 M_s}{2}\begin{pmatrix} -k\sigma(k)-1 & 0 & 0 \\ 0 & -\sigma(k)\frac{k_y^2}{k} & -\sigma(k)\frac{k_yk_z}{k} \\ 0 & -\sigma(k)\frac{k_yk_z}{k} & -\sigma(k)\frac{k_z^2}{k} \end{pmatrix}\mathbf{m}(\mathbf{k}). \tag{3.72}$$

Using the same steps as before the susceptibility matrix is deduced.

Dispersion relation

Looking at the magnetization transverse to the equilibrium position. Still considering $m_z = \sqrt{1-m_x^2-m_y^2} \sim 1$

$$\begin{aligned} -i\omega m_x &= -\gamma(m_yB_z - B_ym_z) + i\omega\alpha m_y \\ -i\omega m_y &= -\gamma(B_xm_z - m_xB_z) - i\omega\alpha m_x \end{aligned} \tag{3.73}$$

Where

$$\begin{aligned} \gamma B_x &= \frac{\omega_{\mathrm{ex}}}{4\gamma}\left(k^2-\kappa_n^2\right)m_x - \frac{\omega_D}{2}\left(k\sigma(k)+1\right)m_x + \gamma B_{AC,x} \\ \gamma B_y &= \frac{\omega_{\mathrm{ex}}}{4\gamma}\left(k^2-\kappa_n^2\right)m_y - \frac{\omega_D}{2}\left(\sigma(k)\frac{k_y^2}{k}m_y + \sigma(k)\frac{k_yk_z}{k}m_z\right) + \gamma B_{AC,y} \\ \gamma B_z &= \omega_0 + \frac{\omega_{\mathrm{ex}}}{4\gamma}\left(k^2-\kappa_n^2\right)m_z - \frac{\omega_D}{2}\left(\sigma(k)\frac{k_yk_z}{k}m_y + \sigma(k)\frac{k_z^2}{k}m_z\right) \end{aligned} \tag{3.74}$$

In the linear regime we neglect higher order terms like m_x^2, m_y^2, m_z^2 and m_ym_x yielding the following equations

$$\begin{aligned} -i\omega m_x &= -\omega_0 m_y + \frac{\omega_D}{2}\left(\sigma(k)\frac{k_z^2}{k}m_y - \sigma(k)\frac{k_y^2}{k}m_y\right) + \gamma B_{AC,y} + i\omega\alpha m_y \\ -i\omega m_y &= \omega_0 m_x + \frac{\omega_D}{2}\left(\left(k\sigma(k)+1\right)m_x - \sigma(k)\frac{k_z^2}{k}m_x\right) + \frac{\omega_{\mathrm{ex}}k^2}{2}m_x - \gamma B_{AC,x} - i\omega\alpha m_x \end{aligned} \tag{3.75}$$

$$\begin{aligned} -i\omega m_x + m_y\left(\omega_0 - \frac{\omega_D}{2}\left(\sigma(k)\frac{k_z^2}{k} - \sigma(k)\frac{k_y^2}{k}\right) - i\omega\alpha\right) &= \gamma B_{AC,y} \\ -i\omega m_y + m_x\left(-\omega_0 - \frac{\omega_D}{2}\left(k\sigma(k)+1-\sigma(k)\frac{k_z^2}{k}\right) - \frac{\omega_{\mathrm{ex}}k^2}{2} + i\omega\alpha\right) &= -\gamma B_{AC,x} \end{aligned} \tag{3.76}$$

Defining the following

$$\begin{aligned} \omega_2' &= \omega_0 + \frac{\omega_{\mathrm{ex}}k^2}{2} + \frac{\omega_D}{2}\left(k\sigma(k)+1-\sigma(k)\frac{k_z^2}{k}\right) \\ \omega_3' &= \omega_0 - \frac{\omega_D}{2}\left(\sigma(k)\frac{k_z^2}{k} - \sigma(k)\frac{k_y^2}{k}\right) \end{aligned} \tag{3.77}$$

we get the same form as in chapter 3.1 from which we want to exclude the susceptibility $\mathbf{m} = \chi \mathbf{B}_{AC}$:

$$\begin{pmatrix} \omega_2' - i\alpha\omega & i\omega \\ -i\omega & \omega_3' - i\alpha\omega \end{pmatrix} \begin{pmatrix} m_x \\ m_y \end{pmatrix} = \gamma \begin{pmatrix} B_{AC,x} \\ B_{AC,y} \end{pmatrix} \tag{3.78}$$

.

$$\chi' = \frac{\gamma}{(\omega_2' - i\alpha\omega)(\omega_3' - i\alpha\omega) - \omega^2} \begin{pmatrix} \omega_3' - i\alpha\omega & -i\omega \\ i\omega & \omega_2' - \alpha\omega \end{pmatrix} \tag{3.79}$$

Solving for the singularities:

$$\omega = -i\alpha \frac{(\omega_2 + \omega_3)}{2(1+\alpha^2)} \pm \sqrt{\frac{\omega_2\omega_3}{1+\alpha^2} - \frac{\alpha^2(\omega_2+\omega_3)^2}{4(1+\alpha^2)^2}} \tag{3.80}$$

In YIG the damping is very small ($\alpha << 1$) therefore we neglect α^2 terms:

$$\omega_{sw}' \approx \sqrt{\omega_2'\omega_3'} \tag{3.81}$$

The dispersion relations for the unpinned and pinned situations plotted against the 2D relations computed in the earlier chapter are given in figure 3.6.

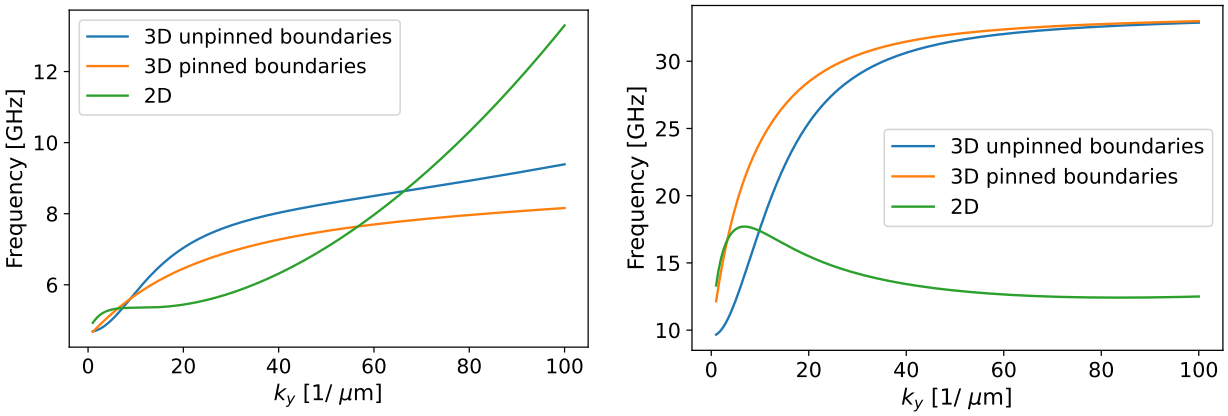

Figure 3.6: **Calculated spin wave dispersion for YIG (on the left) and for Permalloy (on the right)**. Calculation made for a film of 235nm thick with saturation magnetization $M_s = 1.42 \times 10^5$ A/m. The external magnetic field is taken to be B=100mT. All the calculations methods shown in the paper are represented here; 2D (or without taking the transversal modes into consideration) and 3D pinned (from section 3.2.1) and unpinned (from section 3.2.2).

3.3. Efficiency of the generation of spin waves

The spin waves in the sample are excited by application of an oscillating current through a narrow strip-line embedded in the sample. Due to Oersted's law, this oscillating current generates an oscillating magnetic field at microwave frequencies. The magnetic field generated by the strip line is deduced in this section. This magnetic field couples to the spins in the YIG which start precessing and spin waves are excited at the frequency of the oscillating magnetic field. In this section it is deduced that only spin-waves with certain values of $\mathbf{k}$ can be excited efficiently. A current is sent through the strip-line in the z direction with current density $\mathbf{J}(\mathbf{r})$. Ref. [9] gives the magnetic field as created by the current going through the strip-line of volume V using the Biot-Savart law

$$\mathbf{B}(\mathbf{r}) = \frac{\mu_0}{4\pi} \int_V \frac{\mathbf{J}(\mathbf{r}') \times (\mathbf{r} - \mathbf{r}')}{|\mathbf{r} - \mathbf{r}'|^3} d\mathbf{r}' = \frac{\mu_0}{4\pi} \int_V \mathbf{J}(\mathbf{r}') \times -\nabla \left(\frac{1}{|\mathbf{r} - \mathbf{r}'|} \right) d\mathbf{r}' = \frac{\mu_0}{4\pi} \nabla \times \int_V \frac{\mathbf{J}(\mathbf{r}')}{|\mathbf{r} - \mathbf{r}'|} d\mathbf{r}' \tag{3.82}$$

Now since $\mathbf{B} = \nabla \times \mathbf{A}$, we can derive the magnetization vector potential

$$\mathbf{A}(\mathbf{r}) = \frac{\mu_0}{4\pi} \int_V \frac{\mathbf{J}(\mathbf{r}')}{|\mathbf{r} - \mathbf{r}'|} d\mathbf{r}' \tag{3.83}$$

We now consider the more general case where the current is time dependent, taking into account the arrival time of the electromagnetic 'message' we get the retarded potential as given by [7].

$$\mathbf{A}(\mathbf{r},t) = \frac{\mu_0}{4\pi}\int_V \frac{\mathbf{J}(\mathbf{r}',t_r)}{|\mathbf{r}-\mathbf{r}'|}\mathrm{d}\mathbf{r}' \tag{3.84}$$

which included the retarded time $t_r \equiv t - \frac{|\mathbf{r}-\mathbf{r}'|}{c}$, c being the speed of light. This permits the step to the frequency domain:

$$\mathbf{A}(\mathbf{r},\omega) = \frac{\mu_0}{4\pi}\int_V \frac{\mathbf{J}(\mathbf{r}',\omega)e^{ik|\mathbf{r}-\mathbf{r}'|}}{|\mathbf{r}-\mathbf{r}'|}\mathrm{d}\mathbf{r}' \tag{3.85}$$

In our experiments, we consider a microstrip of width w, length l and thickness δ the current flowing in the direction of the external magnetic field, in the z direction. This implies $\mathbf{A} = A\hat{\mathbf{z}}$ and therefore $B_z = 0$. The microwave field can now be deduced using the definition of $\mathbf{A}$, assuming the current density is homogeneous.

$$\begin{pmatrix} B_x \\ B_y \\ B_z \end{pmatrix} = \begin{pmatrix} \frac{\partial A_z}{\partial y} \\ -\frac{\partial A_z}{\partial x} \\ 0 \end{pmatrix} \tag{3.86}$$

Using Weyl's identity [3] we find

$$A_z(x,y,z) = \frac{\mu_0 J(\omega)}{4\pi}\int_{\frac{-\delta}{2}}^{\frac{\delta}{2}}\mathrm{d}x'\int_{\frac{-w}{2}}^{\frac{w}{2}}\mathrm{d}y'\int_{\frac{-l}{2}}^{\frac{l}{2}}\mathrm{d}z'\frac{e^{ik|\mathbf{r}-\mathbf{r}'|}}{|\mathbf{r}-\mathbf{r}'|} \tag{3.87}$$

$$A_z(x,y,z) = \frac{\mu_0 J(\omega)}{4\pi}\int_{\frac{\delta}{2}}^{\frac{\delta}{2}}\mathrm{d}x'\int_{\frac{-w}{2}}^{\frac{w}{2}}\mathrm{d}y'\int_{\frac{-l}{2}}^{\frac{l}{2}}\mathrm{d}z'\frac{i}{2\pi}\int\mathrm{d}k_y\mathrm{d}k_z\frac{e^{ik_x|x-x'|+ik_y(y-y')+ik_z(z-z')}}{k_x} \tag{3.88}$$

$$A_z(x,k_y,k_z) = \frac{\mu_0 J(\omega)}{2}\int_{\frac{-\delta}{2}}^{\frac{\delta}{2}}\mathrm{d}x'\int_{\frac{-w}{2}}^{\frac{w}{2}}\mathrm{d}y'\int_{\frac{-l}{2}}^{\frac{l}{2}}\mathrm{d}z'\frac{e^{ik_x|x-x'|-ik_y y'-ik_z z'}}{k_x} \tag{3.89}$$

where $k_x = \sqrt{k^2-k_y^2-k_z^2}$ and $k = \omega/c$. Computing the integrals gives

$$A_z(x,k_y,k_z) = 2i\mu_0 J(\omega)\frac{e^{-ik_x x}(e^{ik_x\delta}-1)}{k_x^2 k_z k_y}\sin\frac{k_y w}{2}\sin\frac{k_z l}{2}e^{-ik_z z_i} \tag{3.90}$$

from which we can deduce using 3.86 that

$$B_x(x,k_y,k_z) = 2i\mu_0 J(\omega)\frac{e^{-ik_x x}(e^{ik_x\delta}-1)}{k_x^2 k_z}\sin\frac{k_y w}{2}\sin\frac{k_z l}{2}e^{-ik_z z_i} \tag{3.91}$$

$$B_y(x,k_y,k_z) = -2i\mu_0 J(\omega)\frac{e^{-ik_x x}(e^{ik_x\delta}-1)}{k_x k_y k_z}\sin\frac{k_y w}{2}\sin\frac{k_z l}{2}e^{-ik_z z_i} \tag{3.92}$$

With z_i the center of the strip line. The generated magnetic field is perpendicular to the axis of the strip line. Also since the strip line is much longer than wide ($l >> w$) the oscillations are quickest from the second sinus term in the equations of the magnetic field. In our experiments we can assume $k_x = \sqrt{k^2-k_y^2-k_z^2} \approx i\sqrt{k_y^2+k_z^2} \equiv i\kappa$ leading to :

$$B_x(x,k_y,k_z) = -2i\mu_0 J(\omega)\frac{e^{\kappa x}(e^{-\kappa\delta}-1)}{\kappa^2 k_z}\sin\frac{k_y w}{2}\sin\frac{k_z l}{2}e^{-ik_z z_i} \tag{3.93}$$

$$B_y(x,k_y,k_z) = -2\mu_0 J(\omega)\frac{e^{\kappa x}(e^{-i\kappa\delta}-1)}{\kappa k_y k_z}\sin\frac{k_y w}{2}\sin\frac{k_z l}{2}e^{-ik_z z_i} \tag{3.94}$$

From theses equations we can deduce that not every wavelength of spin waves can be efficiently generated by the strip line as can be seen in figure 3.7.when an integer number of wavelengths fits under the microstrip width ($k = n*2\pi/w$) the excitation efficiency vanishes. In figure 3.4 the dispersion relations for YIG and Permalloy are plotted with the x-axis limited by the first integer amount of the strip line width.

[3] The Weyl identity is $\frac{e^{ik|\mathbf{r}-\mathbf{r}'|}}{|\mathbf{r}-\mathbf{r}'|} = \frac{i}{2\pi}\int\mathrm{d}k_y\mathrm{d}k_z\frac{e^{ik_x|x-x'|+ik_y(y-y')+ik_z(z-z')}}{k_x}$

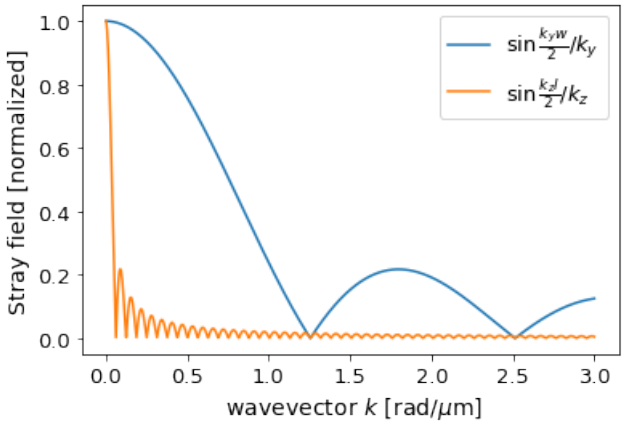

Figure 3.7: **Effect of the strip line shape and dimensions of the generated spin waves**. A strip line of thickness $w = 5\mu m$ and length $l = 100\mu m$ can generate spin waves with large k_y but not large k_z

In our experiments the polarization of the spin waves is of importance because [2] shows that ESR transitions are driven by circularly polarized magnetic fields. Depending on the polarization they drive either $m_s = 0$ to $m_s = -1$ ESR transitions or $m_s = 0$ to $m_s = +1$ ESR transitions. Thus to be measured correctly the magnetic field the spin-waves generate need to be circularly polarized. Notice the relation $B_x = ik_y B_y/\kappa$. When in the backward volume regime ($|k_y| << |k_z|$) this relation becomes $|B_y| << |B_x|$ so the field becomes linearlised in the x direction. But in the Damon-Eshbach regime ($|k_z| << |k_y|$) the relation becomes $B_x = iB_y$ which represents a circularly polarized spin wave field. The stray field created by the spin waves above the YIG sample, in the diamond which is therefore measured by the NV centers is also computed in [2]. For the DE regime this is also circularly polarized but of opposite handedness.

In conclusion the right propagating ($+k_y$) DE spin waves which we measure in our experiments create a stray field in the diamond which is left circularly polarized and therefore drives the $m_s = 0$ to $m_s = -1$ ESR transitions.

4

Experimental results

4.1. Experimental setup

During this project I assisted a few lab sessions where we tried to fix issues with the measuring setup. The purpose of the measurements where to broaden the accessible frequencies of the measured spin waves using AC magnetometry and the difference frequency generation method. Our experimental setup consist of a YIG sample into which gold striplines are embedded in order to generate the spin waves in the material. Our magnetometer is a diamond chip with a high density of NV centers which is placed at a distance of approximately 1 µm from the sample. A green laser is shined on the diamond sample to initiate the NV centers in the $m_s = 0$ and generate the needed PL to do the measurements.

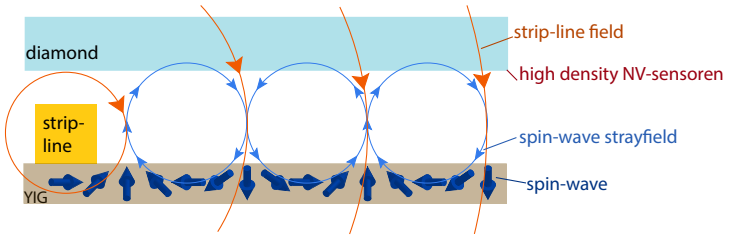

Figure 4.1: **Schematization of the positions of the sample, the golden strip-line and the diamond containing NV centers**. The strip-line generates a magnetic field that inductively starts the precession of the spins in the YIG sample. The spins generate their own circularly polarized strayfield which gets detected by the NV centers in the diamond above.

4.2. Confocal microscope

The setup used in the measurements that where made is a custom-build confocal microscope. Here we give a simple overview of the setup and it's components.
A 515nm laser is used to initialise the NV in the diamond like shown in 4.2. To get the fastest possible modulation of the light an acousto-optic modulator (AOM) is used. Scanning mirrors are used to position the light on the sample, these are controlled by the graphical user interface showed in 4.3. An objective focuses the light beam on the sample and the diamond containing the NV centers. A dichroic mirror divides the incoming green light from the red light returning from the sample. The red PL photons coming from the NV centers are detected using two avalanche photon detectors (APD) to allow for higher counts without surpassing the maximum intensity. Before getting to the APD the light is filtered a last time to remove the remaining green photons and split equally to the two APD's. Throughout the light's parkour there are items correcting the light's polarisation because the efficiency of the excitation of the NV centers is best when the polarisation is aligned with the looked at NV center family.

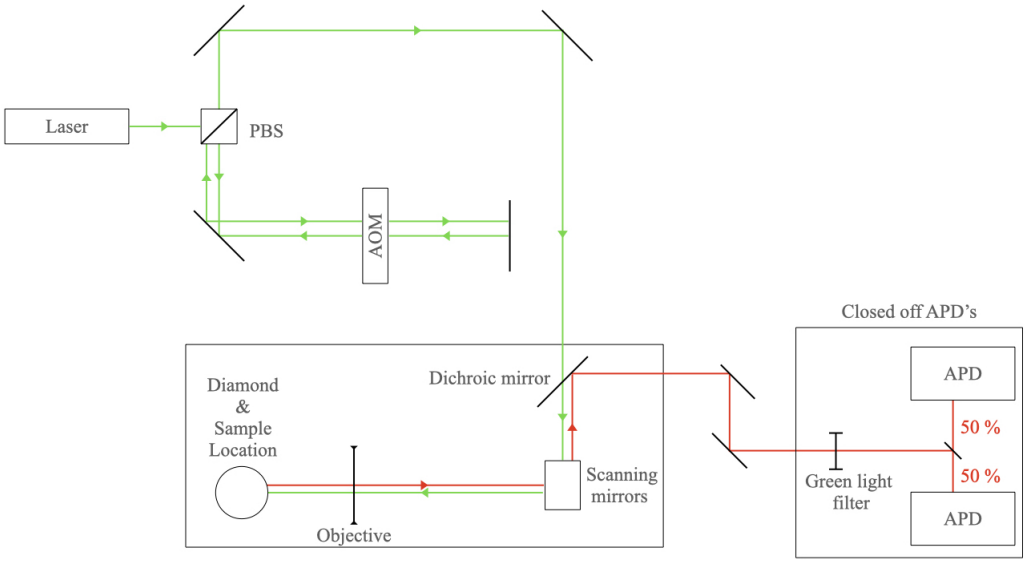

Figure 4.2: **Simplified schematisation of the experimental setup**. A few interposed pinholes and lenses improving the laser path and plates correcting the light polarisation where removed from this image to simplify it.

4.3. Steps of the measurement scheme

The measurements made during this project are a combination of the difference-frequency generation method and AC magnetometry.

A location on the YIG sample is chosen and measurements are made there, this is done using the Graphical user interface presented in figure 4.3. This image also shows an NV scan of the YIG sample, the stripline is apparent in red and the rest of the sample is blue.

To start the measurements the ESR frequency for the currently applied static magnetic field needs to be determined, a simple ESR sweep is done and fitted to find it. The static magnetic field chosen during the measurements made below is $B = 376$G which resulted in an ÈSR frequency of $f_{NV} = 1.817$GHz.

To start the measurements the Bloch sphere rotations needed to perform the AC magnetometry pulse scheme (the π and $\pi/2$ pulses) need to be calibrated by measuring the Rabi oscillations frequency. A Rabi oscillation is shown in 4.4. After the pulses have been calibrated an AC magnetometry measurement as described in section 2.2.3 can be performed. The results of this are shown in figure 4.5. Here we used a XY4 pulse sequence, which consists of two π_X pulses interleaved with two π_Y pulses. With a final $+\pi/2$ pulse (which results in the $m_s = 0$ state when no oscillating field is present)or $-\pi/2$ pulse (which results in the $m_s = -1$) before readout. In figure 2.5 a clear contrast is observable which attest that the spin has a maximal phase difference. The frequency of the applied oscillating magnetic field was $f = 1.25$MHz. This measurement validates the AC magnetometry method since the collapse in figure 2.5 is visible at $\tau = 200$ns. The interpulse time between the π pulses being 2τ, the theory predicts the collapse at $\tau = T/4 = 200$ns with T the period of the oscillating field.

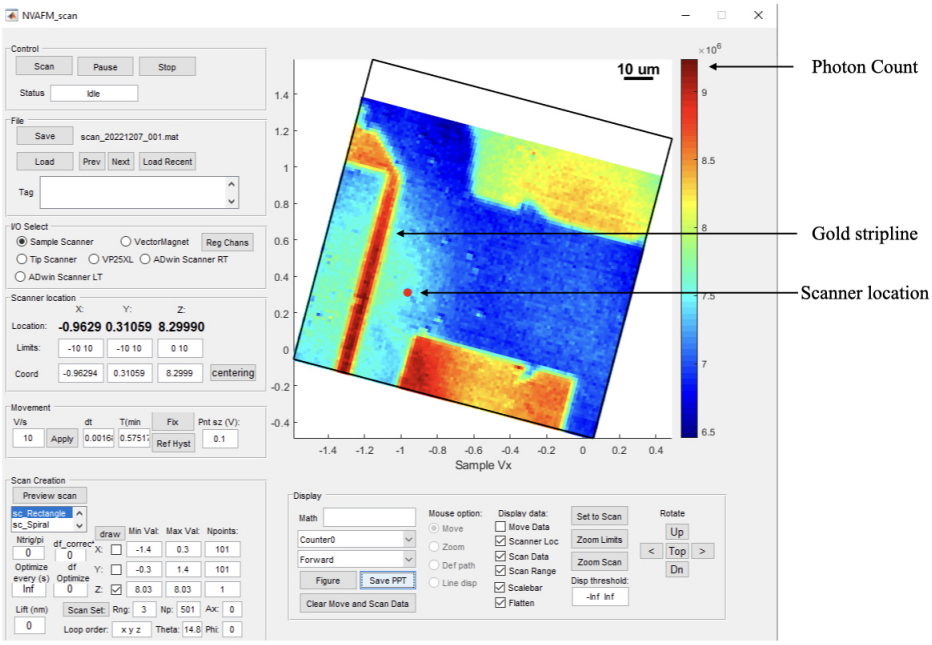

Figure 4.3: **Screenshot of the GUI positioning the scanner on the sample**. The 'Scanner location' indicates where the red dot on the sample is located and where the NV measurements will take place. The image on the right is an NV scan of the sample; which measured the PL counts as a function of their location (which is given in Volts). On the image the gold stripline in apparent on the blue background which is the YIG sample.

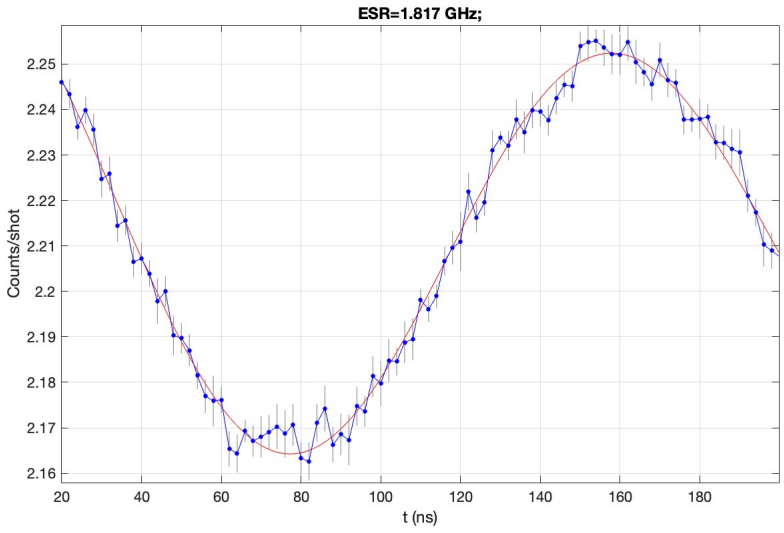

Figure 4.4: **Rabi oscillations measurements**. Measurement made to calibrate the π pulses needed for the AC magnetometry scheme. On the y axis is the measured PL and on the x axis is the length of the microwave pulse applied. The length of a π pulse can here be deduces from the period.

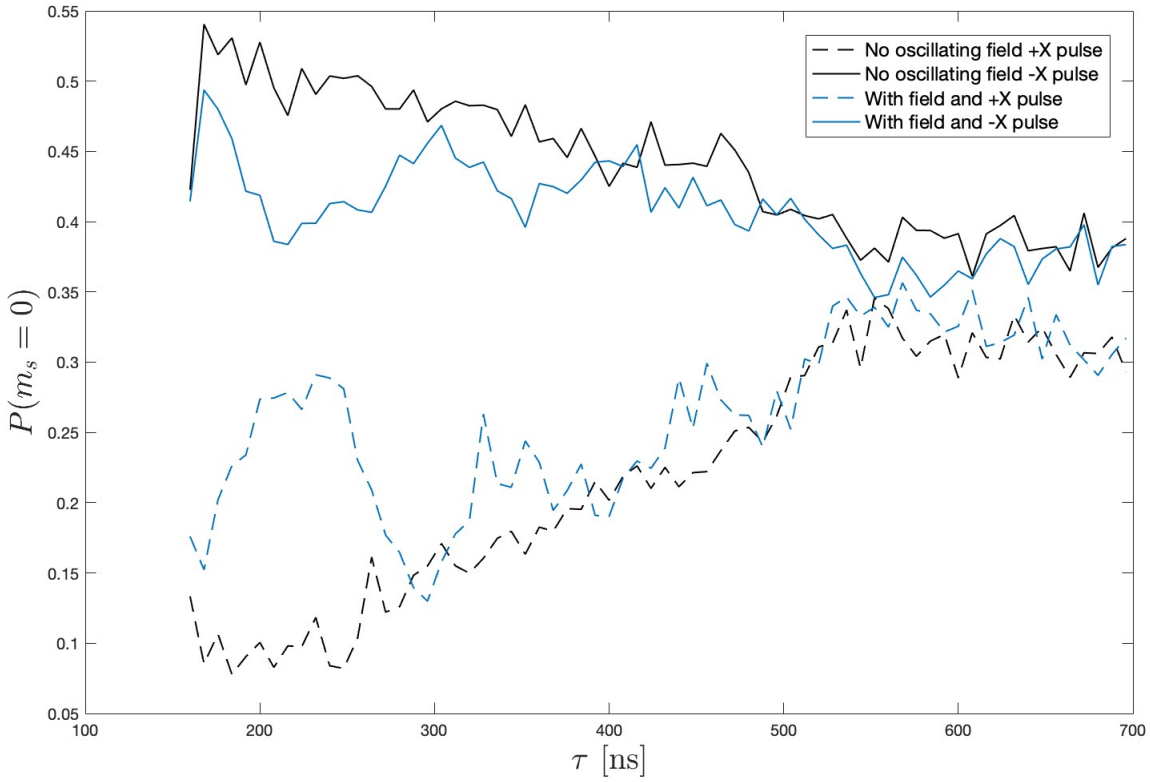

Figure 4.5: **AC magnetometry measurement**. On the y axis the probability that the NV centers are in the $m_S = 0$ state after readout this is inferred from the measured PL. On the x-axis the time passed between the π pulses. The black lines are the reference lines, measured without oscillating magnetic field. The blue lines are with oscillating magnetic field. The upper lines have a final $+\pi/2$ pulse and the lowr lines a $-\pi/2$ pulse. A contrast is observable around 200ns.

5

Outlook

To see whether our analysis of the dispersion relation taking into account the perpendicular modes was successful we can compare it to the calculations made by Kalinikos and Slavin in [10]. Their calculations for the $n = 0$ mode give the results shown in figure 5.1. The magnetic field used for these calculations in unclear but it gives an indication on how the curves should look. In the geometry of this project the angle θ between the normal of the sample and the magnetic field is 90ř as situation A in 5.1. The curves from our derived equations look very different. The next goals for the dispersion relation was to generalize to higher order modes within

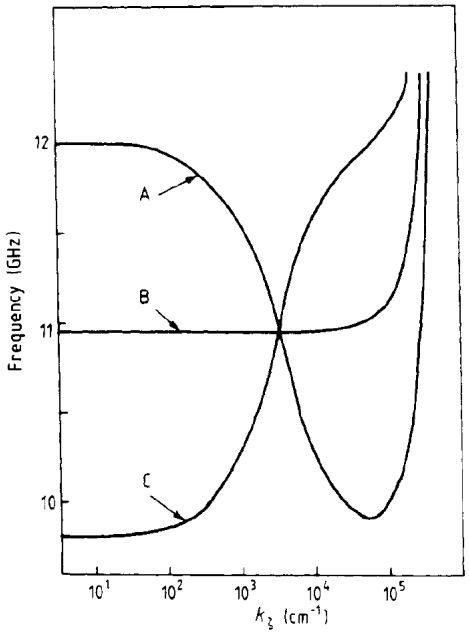

Figure 5.1: **Dispersion relations plotted in the paper by Kalinikos**. Image taken from [10].Dispersion curves for the lowest spin wave eigen-wave (n = 0) propagating in the film with totally unpinned surface spins along the projection of the bias magnetic field. Different curves correspond to the different polar angles 8: (A), 90"; (B), 45"; (C), 0"; between the film normal and the bias magnetic field (see figure 1). Sample with thickness 5 pm and pinned spin surfaces.

the thickness of the sample, this means finish the calculations with κ_n and the following assumption

$$\mathbf{m}(x,\mathbf{k}) = \begin{cases} \mathbf{m}(\mathbf{k})\cos(\kappa_n x) & \text{for } -h < x < 0 \\ 0 & \text{elsewhere .} \end{cases} \tag{5.1}$$

And then compare them to the higher order results from [10]. The first order mode was apparent in the measurements but it would have been interesting to see if higher modes could be measured experimentally. Next step would have been to see how the modes, n and n', interact with each-other. For instance taking the overlap

between the demagnetizing field of two modes, changing equation 3.69 into

$$\overline{\mathbf{B_D}(\mathbf{k})} = \frac{\mu_0 M_s}{h} \int_{-h}^{0} \int_{-h}^{0} \Gamma\left(x - x', \mathbf{k}\right) \cos\left(\kappa_{n'} x'\right) \mathrm{d}x' \cos\left(\kappa_n x\right) \mathrm{d}x \mathbf{m}(\mathbf{k}) \tag{5.2}$$

As to the experimental part of this project, the next step would have been to try to analyse the data accumulated in figure 2.5 and try to quantify the magnetic field we where trying to detect by understanding the exact computations of the relation between the contrast that is observed in figure 2.5 and the oscillating magnetic field.
One of the goals described in the project description was to start measurements using a new material as sample: Permalloy. The interest of Permalloy would have been it's conductive properties. The golden strip for instance could not be embedded directly onto the Permalloy sample since it has a conductance, it was placed at a 5µm distance from the sample. This raises the question of whether the spin waves could even be generated and detected from this sample.

6

Conclusion

In this project we looked at the underlying theory of spin waves in ferromagnetic materials. Considering the geometry of our experiments there are conditions which the microwaves need to satisfy in order to efficiently generate spin-waves in our sample and to be able to detect them properly. If an integer number of wavelengths fits under the microstrip width the efficiency vanishes. We need to generate a circularly polarized magnetic field to properly drive the ESR transitions needed to detect the field. The correctly polarized waves are generated in the Demon-Eshbach regime, thus for waves propagating in the $+y$ direction (to the 'right' of the stripline).

The dispersion relation for a 2D situation, not taking into account the transversal modes was computed and gave the following result:

$$\omega_{\text{sw}} = \sqrt{\left(\omega_1 + f\omega_D\right)\left(\omega_1 + (1-f)\omega_D\right)} \tag{6.1}$$

with variables defined as in equations 3.20. An attempt to add to the model was made by considering the modes appearing in the thickness of the sample in the calculations of the dispersion relation which gave for unpinned spin edges:

$$\omega'_{\text{sw}} \approx \sqrt{\omega'_2\omega'_3} \tag{6.2}$$

with variables as defined in equations 3.77. For pinned edges the dispersion was given by

$$\omega'_{\text{sw}} \approx \sqrt{\omega'_2\omega'_3 + \omega'^2_1} \tag{6.3}$$

with variables defined as in equations 3.51.
The experimental setup was detailed and the steps of an AC measurement where presented. The theory of this method predicted a contrast in probability to find the spin in the $m_s = 0$ state between the situation with oscillating magnetic field and without at a certain interpulse time. This contrast was apparent in the measurements and was at the expected time location. This results makes AC magnetometry a successful method to be used in further experiments. For instance to be tried out with the Permalloy sample.

References

[1] Nitrogen-vacancy center, Jan 2023. URL https://en.wikipedia.org/wiki/Nitrogen-vacancy_center.

[2] Iacopo Bertelli. *Magnetic imaging of spin waves and magnetic phase transitions with nitrogen-vacancy centers in diamond*. PhD thesis, Leiden University, 2021.

[3] Iacopo Bertelli, Brecht G. Simon, Tao Yu, Jan Aarts, Gerrit E. Bauer, Yaroslav M. Blanter, and Toeno Sar. Imaging spin-wave damping underneath metals using electron spins in diamond. *Advanced Quantum Technologies*, 4(12):2100094, 2021. doi: 10.1002/qute.202100094.

[4] A. V. Chumak, V.nbsp;I. Vasyuchka, A.nbsp;A. Serga, and B. Hillebrands. Magnon spintronics, Jun 2015. URL https://www.nature.com/articles/nphys3347/.

[5] G. de Lange, D. Ristè, V. V. Dobrovitski, and R. Hanson. Single-spin magnetometry with multipulse sensing sequences. *Phys. Rev. Lett.*, 106:080802, Feb 2011. doi: 10.1103/PhysRevLett.106.080802. URL https://link.aps.org/doi/10.1103/PhysRevLett.106.080802.

[6] T. Gilbert. A phenomenological theory of damping in ferromagnetic materials: Semantic scholar, Jan 1970. URL https://www.semanticscholar.org/paper/A-phenomenological-theory-of-damping-in-materials-Gilbert/28ef7b88d387e97791a5d579e108bc8cf6c5ccb9.

[7] David J. Griffiths. *Introduction to electrodynamics*. Cambridge University Press, 2019.

[8] Konstantin Y. Guslienko and Andrei N. Slavin. Magnetostatic green's functions for the description of spin waves in finite rectangular magnetic dots and stripes. *Journal of Magnetism and Magnetic Materials*, 323 (18):2418–2424, 2011. ISSN 0304-8853. doi: https://doi.org/10.1016/j.jmmm.2011.05.020. URL https://www.sciencedirect.com/science/article/pii/S0304885311002897.

[9] Umran S. Inan and Aziz S. Inan. *Engineering electromagnetics*. Addison-Wesley, 1999.

[10] B A Kalinikos and A N Slavin. Theory of dipole-exchange spin wave spectrum for ferromagnetic films with mixed exchange boundary conditions. *Journal of Physics C: Solid State Physics*, 19(35):7013, dec 1986. doi: 10.1088/0022-3719/19/35/014. URL https://dx.doi.org/10.1088/0022-3719/19/35/014.

[11] Sergio M. Rezende. *Spin Waves in Ferromagnets: Semiclassical Approach*, pages 31–70. Springer International Publishing, Cham, 2020. ISBN 978-3-030-41317-0. doi: 10.1007/978-3-030-41317-0_2. URL https://doi.org/10.1007/978-3-030-41317-0_2.

[12] Romana Schirhagl, Kevin Chang, Michael Loretz, and Christian L. Degen. Nitrogen-vacancy centers in diamond: Nanoscale sensors for physics and biology. *Annual Review of Physical Chemistry*, 65(1):83–105, 2014. doi: 10.1146/annurev-physchem-040513-103659.

A

Appendix

A.1. Table of definitions

Constants		
Notation	**Definition**	**Description**
γ		Electron gyromagnetic ratio
α_G		Gilbert damping
μ_0		Magnetic permeability
M_s		Saturation magnetization
D		Zero field splitting of the ground state of the NV center
$D_e x$		Zero field splitting of the excited state of the NV center
Ω_R		Rabi frequency
ω_{ex}	$\gamma D / M_s$	
ω_{D}	$\gamma \mu_0 M_s$	
ω_{sw}	depends on the chapter	Spin wave dispersion
Vectors		
Notation	**Definition**	**Description**
$\mathbf{B_0}$		External static magnetic field
$\mathbf{B}_{\text{D}}$		Demagnetizing field
$\mathbf{B}_{\text{Z}}$		Zeemann splitting field
$\mathbf{B}_{\text{ex}}$		Effective field created by the exchange energy
$\mathbf{B}_{\text{AC}}$		Oscillating magnetic field to be detected
$\mathbf{r}$	$\mathbf{r} = x\mathbf{e_x} + y\mathbf{e_y} + z\mathbf{e_z}$	Position vector
$\mathbf{m} = \mathbf{m}(\mathbf{r})$	$\mathbf{m} = m_x\hat{\mathbf{x}} + m_y\hat{\mathbf{y}} + m_z\hat{\mathbf{z}} = \mathbf{M}/M_s$	Normalized magnetization within the sample as function of time and place
$\mathbf{k}$	$\mathbf{k} = k_y\hat{\mathbf{y}} + k_z\hat{\mathbf{z}}$	Wave vector in the sample plane
$\mathbf{J}(\mathbf{r})$		Current density in the strip line
$\mathbf{A}(\mathbf{r})$		magnetization vector potential from the current in the strip line
Energies		
F		Free density energy in the sample
F_Z	See equation 3.5	Zeemann energy density
Functions		
$\Gamma_{\alpha,\beta}(\mathbf{r},\mathbf{r}')$		Coulomb kernel
Fourrier transforms		
$\mathbf{f}(x,\mathbf{k})$		2D spatial fourrier transform over the sample plane
$\Gamma_{\alpha,\beta}(x,\mathbf{k})$		Coulomb kernel Fourrier transformed onto the yz plane